

Segmentation of Bias Field Induced Brain MR Images Using Rough Sets and Stomped- t Distribution

Abhirup Banerjee^{a,b,1}, Pradipta Maji^{c,*}

^aRadcliffe Department of Medicine, Division of Cardiovascular Medicine, University of Oxford, Oxford, United Kingdom.

^bDepartment of Engineering Science, Institute of Biomedical Engineering, University of Oxford, Oxford, United Kingdom.

^cBiomedical Imaging and Bioinformatics Lab, Machine Intelligence Unit, Indian Statistical Institute, Kolkata, India.

Abstract

Over the past few decades, automatic segmentation of brain magnetic resonance (MR) images into different tissue classes has remained an important research area, particularly due to the presence of bias field artifact in MR images. In this regard, the stomped normal (StN) distribution is proved to generate an optimal representation of the intensity distribution in brain MR images, by incorporating the properties of rough sets in the probabilistic framework. The StN distribution is capable of successfully modelling the central tendency, dispersion, and width of the intensity distribution. However, it does not take into consideration the kurtosis of the distribution, which controls the concentration of values around the mean and shape of the tail of intensity distribution. In this regard, the paper presents a novel method for simultaneous segmentation and bias field correction in brain MR images. It integrates the concept of rough sets and the merit of a recently introduced probability distribution, called stomped- t (St- t) distribution. The St- t distribution incorporates the property of kurtosis in rough-probabilistic framework, where each tissue class is modelled using a crisp lower approximation and a probabilistic boundary region. The brain MR image is modelled using a mixture of finite number of St- t distributions and one uniform distribution. The uniform distribution takes into account cerebro-spinal fluid, pathologies, and other non-brain tissues. The proposed method employs both expectation-maximization algorithm and hidden Markov random field model for accurate and robust image segmentation. The performance of the proposed approach, along with a comparison with related methods, is illustrated on a set of synthetic and real brain MR images for different bias fields and noise levels.

Keywords: Stomped- t distribution, rough sets, segmentation, brain MR images, bias field correction, hidden Markov random field.

1. Introduction

Segmentation is often required at a preliminary stage of medical image analysis for computer-aided diagnosis and therapy. It is an indispensable process in the visualization of human tissues, particularly during clinical analysis of brain images. But, the intrinsic nature of the brain makes this procedure much difficult and challenging. Hence, in medical imaging, accurate segmentation of the brain structure into its three main tissue types, namely, white matter (WM), gray matter (GM), and cerebro-spinal fluid (CSF), has gained significant amount of research attention in past few decades [10, 15, 19]. Brain image segmentation is essential for many diagnostic studies. For example, in multiple sclerosis diseases, accurate quantification of WM lesions is necessary for drug treatment assess-

ment; while in schizophrenia and epilepsy, volumetric analysis of WM, GM, and CSF is required to distinguish the morphological differences between subjects. In cancer treatment, precise delineation of tumor, edema, and necrotic tissues from brain MR images plays a crucial part in prescribing the appropriate therapy. Also, accurate quantification of the tumor facilitates the radiation therapist to optimize the maximal dose to the tumor with minimal radiation to the surrounding normal tissues.

MR imaging (MRI) is an important diagnostic medical image acquisition technique that has the ability to detect, in advance, abnormal growths or alterations in tissues and organs. Hence, significant amount of research in medical imaging involves MR images, specifically due to its precise measurement of soft tissues in a non-invasive and non-radioactive way. One of the important characteristics of brain MR images is that they are mostly piecewise constant with few tissue classes. This unique advantage of brain MR images transforms the process of automated segmentation much simpler and reliable compared to other medical imaging modalities. However, this property does not hold in real life due to the existence of a degrading

*Corresponding author

Email addresses: abhirup.banerjee@cardiov.ox.ac.uk (Abhirup Banerjee), pmaji@isical.ac.in (Pradipta Maji)

¹The work was done when A. Banerjee was a senior research fellow of Machine Intelligence Unit, Indian Statistical Institute, Kolkata.

artifact, commonly known as intensity inhomogeneity or bias field. This specific artifact generates a spatially varying shading effect in MR images and hence, reduces the mean intensity and increases the overall intensity variation in each tissue class; nullifying the property of piecewise homogeneous. This shading artifact generally occurs due to some inherent properties of the MRI device such as static field inhomogeneity, bandwidth filtering of the data, eddy current driven by field gradients, and radio frequency transmission and reception inhomogeneity [30]. However, the shape, position and orientation of imaged object inside the magnet, and some magnetic permeability and dielectric properties of the object can also produce this artifact. Although the artifact is hardly noticeable in human eyes, it can deteriorate the performance of any automated image segmentation technique.

Bias field correction is generally regarded as a necessary preprocessing step that results in better MR image segmentation; whereas accurate segmentation information allows to estimate bias field accurately from the image. Hence, segmentation and bias field correction can be considered as two interdependent techniques. Using these characteristics, simultaneous segmentation and bias field correction methods are developed, where these two procedures are combined to outperform their individual performance and achieve simultaneously better segmentation and inhomogeneity correction. Another important problem in brain MR image segmentation is the uncertainty that occurs due to imprecision in computations and vagueness in class definitions. To address this problem, the concept of granular computing, based on the theory of fuzzy sets [48, 14] and rough sets [40], can be used, as they offer mathematical frameworks to model and propagate uncertainties associated with human cognition process [35].

Rough set theory is an important paradigm to deal with uncertainty, vagueness, and incompleteness. It is proposed for indiscernibility in classification or clustering according to some similarity [40]. It is based on the theory of three-way decisions, which is an extension of the binary-decision model. A tri-partition of a universe consists of three pairwise disjoint subsets whose union is the universe. As a novel and important theory in knowledge discovery, management and utilization, the concept of three-way decisions was first introduced in rough set theory for interpreting the positive, negative, and boundary regions. The use of a tri-partition for knowledge representation, information processing, reasoning, and problem solving has appeared in many disciplines. Recently, the approaches based on a tri-partition of the universe are gaining interest to clustering and image analysis [35]. Lingras and West [29] proposed rough c -means (RCM), where each cluster is represented by a pair of crisp lower and upper approximations. Combining both rough sets and fuzzy sets, Maji and Pal [32] introduced rough-fuzzy c -means (RFCM) and its several variants [33], where each cluster is represented by a crisp lower approximation and a probabilistic and/or possibilistic fuzzy boundary. In order to identify clusters having arbitrary shapes, Maji and Paul [37, 36] proposed robust rough-fuzzy c -means (rRFCM), where the lower approximation of a cluster is possibilistic in nature. Recently, rough set theory has been applied success-

fully in bias field estimation [4] and segmentation of brain MR images [47, 32, 33, 34, 18, 23, 31]. The theory of fuzzy sets has also been extensively used in brain MR image segmentation tasks. Pham and Prince [41] used first and second order regularization terms to model smooth and slowly varying bias field in a fuzzy c -means (FCM) framework. Ahmed et al. [1] introduced a regularization term in the standard FCM framework to compensate for the latent bias field and to tend the solution towards piecewise constant labeling. Several other spatial constraints were subsequently introduced into the FCM framework for robust and improved brain MR image segmentation [22, 16].

The most popular framework to model brain tissue classes for segmentation is the probabilistic model. Ashburner and Friston [2] developed a unified probabilistic framework that combined image registration, tissue classification, and bias field correction within the same generative model. The expectation-maximization (EM) algorithm is used for estimating the maximum likelihood estimate (MLE) of the tissue class parameters in finite Gaussian mixture (FGM) model based brain MR image segmentation [46, 17, 26]. Some spatial constraints are further incorporated into the FGM model for robust image segmentation in noisy environment [38, 13]. The Markov random field (MRF) based techniques have been introduced to incorporate spatial information of the neighboring pixels into the simultaneous segmentation and bias field correction framework [50, 43]. Ji et al. [21] proposed adaptive scale fuzzy local FGM model for robust brain MR image segmentation. Ribbens et al. [42] introduced a data-driven probabilistic framework, which combines segmentation, registration, atlas construction, and clustering of brain MR images in homogeneous subgroups, in a unified framework. Li et al. [28] introduced multiplicative intrinsic component optimization (MICO) technique for simultaneous bias field correction and brain MR image segmentation. Recently, in [8], the intensity distribution of the image classes is modelled using Student's- t distribution for simultaneous brain MR image segmentation and inhomogeneity correction.

The probabilistic frameworks, reported in [46, 17, 26, 38, 13, 50, 43, 21, 42], are based on the normality assumption of tissue classes around mean. The normal or Gaussian distribution, being a unimodal distribution, represents a tissue class using a single intensity value of mean, which, in turn, ensures the definite belongingness of a pixel to the tissue class. In spite of the piecewise constant property of brain MR images, a single intensity value can never represent a tissue class properly. To address the above problem, a new probability distribution, termed as stomped normal (StN) distribution, has been introduced in [5, 6] that is capable of using multiple intensity values to represent a tissue class. The StN distribution models the intensity distribution of each class with the help of its three parameters, namely, mean, variance, and width. But, StN distribution fails to model another important property in the intensity distribution of a class. This property is the degree of peakedness or kurtosis of the intensity distribution, which controls the concentration of values around mean without affecting the standard deviation. To incorporate this very important property of data distribution, recently another new distribution, termed as stomped- t (St- t) distribution [7], has been proposed for modelling data clusters

in rough-probabilistic framework. Its performance has been demonstrated for data clustering, cell delineation, and image segmentation [7]. As the impact of intensity inhomogeneity artifacts on MR images has not been considered, the probabilistic framework of [7] fails to produce the optimal segmented and bias field corrected brain MR images. The probabilistic model of [8] also fails to capture both width and kurtosis parameters of the intensity distribution.

In this regard, the objective of the proposed research work is to introduce the property of kurtosis in rough-probabilistic modelling of tissue classes for brain MR image segmentation. A novel algorithm for simultaneous segmentation and bias field correction of brain MR images, termed as t -StORM, is developed by representing the brain MR image as a finite mixture of St- t distributions and one uniform distribution. The uniform distribution models the CSF, pathologies, and other non-brain tissues. Integration of the concept of rough sets into the St- t distribution enables the algorithm to utilize the advantages of rough clustering with respect to brain MR image segmentation tasks. Each tissue class in brain MR image is modelled using two regions: a crisp lower approximation and a probabilistic boundary. The lower approximation controls the overlapping characteristics of the final tissue class. The proposed algorithm incorporates the advantages of St- t distribution into the joint EM-hidden MRF (HMRF) framework [50] for simultaneous segmentation and bias field correction. The algorithm is generalized in the sense that some of the existing simultaneous segmentation and bias field correction algorithms can be derived from the proposed algorithm as a special case. Moreover, the proposed method introduces a new latent variable to measure the inlierness of each pixel with respect to tissue classes for robust parameter estimation, instead of a pre-specified fixed weight for lower approximation region, as done in [5]. Finally, the efficacy of the proposed algorithm, along with a comparison with related methods, is illustrated on a set of real and simulated brain MR images, both qualitatively and quantitatively for different bias fields and noise levels.

The structure of the rest of this paper is as follows: Section 2 discusses the basic concepts of rough sets. The concepts of StN and St- t distributions are also included in this section. The proposed simultaneous segmentation and bias field correction algorithm is introduced in Section 3. Section 4 demonstrates the performance of the proposed algorithm, along with a comparison with related state-of-the-art methods, for simultaneous segmentation and bias field correction of brain MR images. Concluding remarks are given in Section 5.

2. Basics of Rough Sets, StN and St- t Distributions

This section presents the basic concepts of rough sets, along with two new distributions, namely, StN and St- t . The proposed algorithm for simultaneous bias field correction and brain MR image segmentation is developed based on these concepts.

2.1. Basics of Rough Sets

The theory of rough sets begins with the notion of an approximation space, which is represented as a pair $\langle \mathbb{U}, A \rangle$,

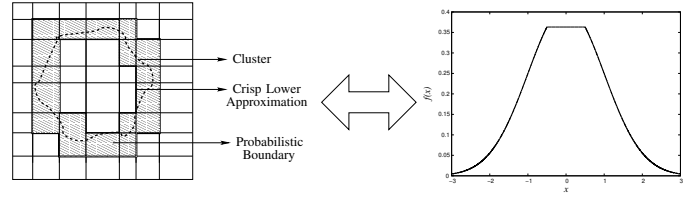


Figure 1. StN distribution incorporates the concepts of lower approximation and boundary region of rough sets.

where $\mathbb{U} = \{o_1, \dots, o_j, \dots, o_n\}$ be a non-empty set, the universe of discourse, and A is an equivalence relation on \mathbb{U} . The relation A partitions the set \mathbb{U} into disjoint classes, so that two elements o_j and o_k belong to the same class iff $(o_j, o_k) \in A$. Let denote by \mathbb{U}/A the quotient set of \mathbb{U} by relation A , and

$$\mathbb{U}/A = \{X_1, \dots, X_i, \dots, X_m\} \quad (1)$$

where X_i represents an equivalence class of A . If two elements o_j and o_k in \mathbb{U} belong to the same equivalence class $X_i \in \mathbb{U}/A$, the elements o_j and o_k are termed as indistinguishable. The equivalence classes of A , along with the empty set \emptyset , are defined as the elementary sets in the approximation space $\langle \mathbb{U}, A \rangle$. Given an arbitrary set $X \in 2^{\mathbb{U}}$, generally, it may not be possible to describe X precisely in $\langle \mathbb{U}, A \rangle$. One may characterize X by a pair of lower and upper approximations defined as [40]

$$\underline{A}(X) = \bigcup_{X_i \subseteq X} X_i; \quad \text{and} \quad \overline{A}(X) = \bigcup_{X_i \cap X \neq \emptyset} X_i. \quad (2)$$

The lower approximation $\underline{A}(X)$ denotes the union of all the elementary sets which are subsets of X , and the upper approximation $\overline{A}(X)$ denotes the union of all the elementary sets which have a non-empty intersection with X . The tuple $\langle \underline{A}(X), \overline{A}(X) \rangle$ is the representation of an ordinary set X in the approximation space $\langle \mathbb{U}, A \rangle$ or simply called the rough set of X . The lower (respectively, upper) approximation $\underline{A}(X)$ (respectively, $\overline{A}(X)$) is defined as the collection of those elements of \mathbb{U} that definitely (respectively, possibly) belong to X . $B(X) = \overline{A}(X) \setminus \underline{A}(X)$ is called the boundary region of X . Further, a set $X \in 2^{\mathbb{U}}$ is said to be definable or exact in $\langle \mathbb{U}, A \rangle$ iff $\underline{A}(X) = \overline{A}(X)$.

2.2. StN Distribution

Gaussian or normal distribution is a unimodal distribution, which possesses highest probability density value at its mean; and the density decreases symmetrically towards its both ends. If a class follows normal distribution, it implies any pixel, belonging to the class, has highest probability of belongingness at the mean value of the distribution and the probability decreases with its deviation from mean. Hence, in case of normal distribution, only the mean intensity value ensures the belongingness of a pixel to the class. However, in reality, there exist multiple intensity values in an image that ensure belongingness of a pixel to a specific class. But, this property is ignored when normal distribution is fitted to model an image class, which, in turn, leads to inaccurate segmentation.

The StN distribution [5] attains highest probability density in a region (lower approximation) around its mean and the probability density decreases (boundary region) while traversing away

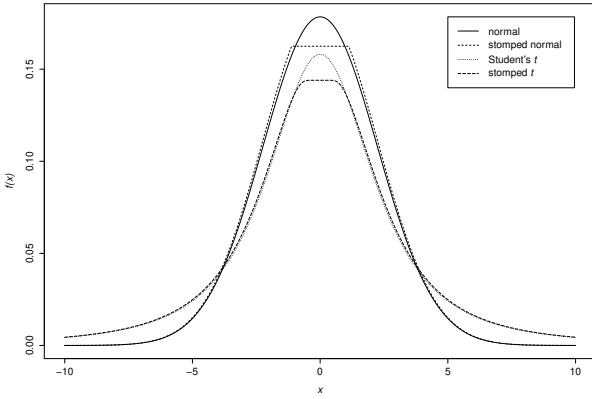


Figure 2. Probability density curves for normal, StN, non-standardized t , and St- t distributions with $\mu = 0$, $\sigma^2 = 5$, $k = 0.5$, and $\nu = 2$.

from the uniform region (Fig. 1). The probability density function (pdf) of StN distribution is given by:

$$f(y; \mu, \sigma^2, k) = \frac{1}{D\sigma} \phi(z), \quad (3)$$

where $z = \begin{cases} k, & \text{if } |\frac{y-\mu}{\sigma}| < k \\ \frac{y-\mu}{\sigma}, & \text{otherwise} \end{cases}$, $D = 2(1 - \Phi(k) + k\phi(k))$, and $\phi()$ and $\Phi()$ are, respectively, the pdf and cumulative distribution function (cdf) of standard normal distribution. In case $k = 0$, Eq. (3) reduces to the pdf of a normal distribution with mean μ and variance σ^2 . Hence, it is clear that the StN distribution is a more generalized probability distribution, whose special case is the Gaussian distribution.

2.3. St- t Distribution

The StN distribution models three important characteristics of data distribution: central tendency, dispersion, and width of the lower approximation region. Apart from these three, there also exists another important characteristics in data that StN distribution fails to model. This property is commonly known as the degree of peakedness or kurtosis of the data distribution, which controls the concentration of values around the mean without affecting the dispersion of data distribution. A high value of kurtosis suggests high concentration of values near mean with smaller tails, which is suitable for modelling piecewise homogeneous brain tissue classes in noise-free environment. Similarly, a lower value of kurtosis suggests low concentration of values near mean with longer tails, which can model even outlier observations in a noisy environment. To incorporate this important characteristic into the StN distribution, the St- t distribution [7] is developed that has the ability to control the kurtosis of the distribution.

In case $Y|U = u \sim StN(\mu, \frac{\sigma^2}{u}, k)$ and $U \sim Gamma(\frac{\nu}{2}, \frac{\nu}{2})$, the pdf of Y is called the pdf of non-standardized St- t distribution with degrees of freedom ν , location parameter μ , and scale parameter σ . For standardized Y with respect to location μ and scale σ , that is, for $X = \frac{Y-\mu}{\sigma}$, the pdf is written as

$$f_X(x) = \frac{1}{D\sqrt{\pi\nu}\Gamma(\frac{\nu}{2})} \left[e^{-\frac{x^2}{2}} \gamma\left(\frac{\nu+1}{2}, \frac{u_0\nu}{2}\right) + \frac{1}{(1+\frac{x^2}{\nu})^{\frac{\nu+1}{2}}} \Gamma\left(\frac{\nu+1}{2}, \frac{u_0}{2}(\nu+x^2)\right) \right], \quad (4)$$

where $u_0 = \frac{k^2}{x^2}$, $\gamma(s, x) = \int_0^x e^{-u} u^{s-1} du$ is the lower incomplete gamma function, and $\Gamma(s, x) = \int_x^\infty e^{-u} u^{s-1} du$ is the upper incomplete gamma function. The above function is defined as the pdf of standardized St- t distribution with ν degrees of freedom.

In case $k = 0$, Y follows non-standardized t -distribution with parameters μ , σ , and ν . As $\nu \rightarrow \infty$, Y becomes marginally StN with parameters μ , σ^2 , and k . Also, in case $\nu \rightarrow \infty$ and $k = 0$, Y follows normal with parameters μ and σ^2 . Fig. 2 compares the probability density curves of normal, StN, non-standardized t , and St- t distributions with parameters $\mu = 0$, $\sigma^2 = 5$, $k = 0.5$, and $\nu = 2$.

3. t -StoRM: Proposed Segmentation Algorithm

This section introduces the t -StoRM algorithm for simultaneous segmentation and bias field correction in brain MR images, integrating the merits of St- t distribution into the joint EM-HMRF framework. A flow-chart of the proposed t -StoRM algorithm is provided in Figure 3.

3.1. Proposed Framework

The bias field is generally modelled as a multiplicative component. If the intensity of the i th pixel of the inhomogeneity-free image is \tilde{v}_i , and corresponding intensity inhomogeneity component and noise are b_i and ϵ_i , respectively, the intensity v_i of the i th pixel of acquired image is obtained as

$$v_i = \tilde{v}_i b_i + \epsilon_i, \quad i \in \mathcal{S} = \{1, \dots, N\}; \quad (5)$$

N being the number of pixels in the image. In general, the bias field is first estimated from the noisy image and then post-filtering is applied to remove noise from the bias corrected image [17]. As the model is multiplicative, a logarithmic transformation is applied on (5) to make the model additive, that is, $y_i = \tilde{y}_i + \beta_i$, where $y_i = \log v_i$, $\tilde{y}_i = \log \tilde{v}_i$, and $\beta_i = \log b_i$. Let x_i be the label of i th pixel and $x_i \in \mathcal{L} = \{1, \dots, l, \dots, L\}$. Y_i and X_i denote, respectively, the random variables of the log-transformed intensity value and class label of the i th pixel of the image. We define a set of latent variables as follows:

$$\delta_{il} = \begin{cases} 1, & \text{if } X_i = l; \\ 0, & \text{otherwise.} \end{cases} \quad (6)$$

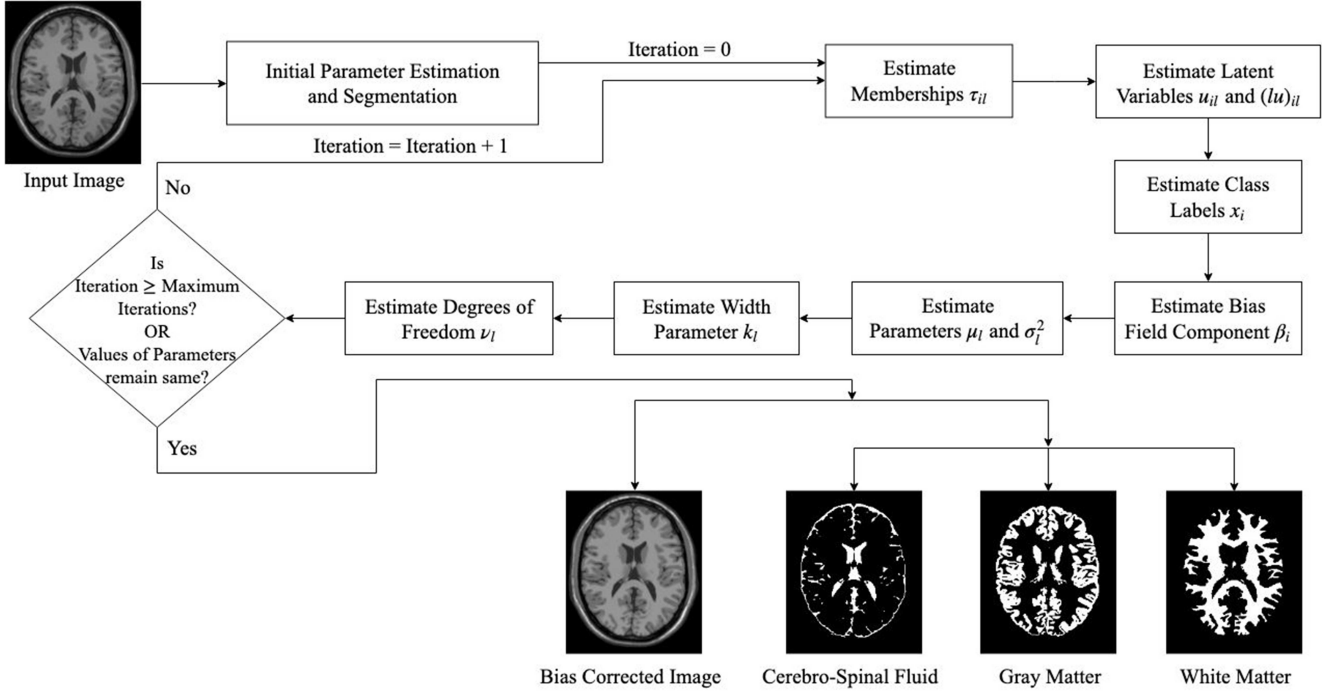
We also assume that the observed data y_i , $i \in \mathcal{S}$ augmented by the δ_{il} , $i \in \mathcal{S}$, $l \in \mathcal{L}$ is still incomplete. So, we introduce a set of additional missing data u_i , $i \in \mathcal{S}$, which are defined so that $Y_i | (U_i = u_i, \delta_{il} = 1, \beta_i) \sim StN(\mu_l, \frac{\sigma_l^2}{u_i}, k_l)$ independently for $i \in \mathcal{S}$ and $U_i | (\delta_{il} = 1) \sim Gamma(\frac{\nu_l}{2}, \frac{\nu_l}{2})$ independently for $i \in \mathcal{S}$. Now,

$$p(y_i | u_i, \delta_{il}, \beta_i) = \frac{\sqrt{u_i}}{D_l \sigma_l} \phi(z_{il}), \quad (7)$$

where $z_{il} = \begin{cases} k_l, & \text{if } \left| \frac{\sqrt{u_i}(y_i - \beta_i - \mu_l)}{\sigma_l} \right| < k_l \\ \frac{\sqrt{u_i}(y_i - \beta_i - \mu_l)}{\sigma_l}, & \text{otherwise} \end{cases}$,

$$D_l = 2(1 - \Phi(k_l) + k_l \phi(k_l)).$$

$$\text{Also, } p(u_i | \delta_{il}) = \left(\frac{\nu_l}{2}\right)^{\frac{\nu_l}{2}} \frac{1}{\Gamma(\frac{\nu_l}{2})} e^{-\frac{\nu_l u_i}{2}} u_i^{\frac{\nu_l}{2}-1} I_{(0, \infty)}(u_i). \quad (8)$$

Figure 3. Flow-chart of the proposed t -StoRM algorithm.

Following the concepts of rough sets, let $\underline{A}(\Omega_l)$ and $B(\Omega_l)$ be the lower approximation and boundary region of the l th tissue class Ω_l . Let, $\bar{A}(\Omega_l) = \{\underline{A}(\Omega_l) \cup B(\Omega_l)\}$ denote the upper approximation of Ω_l . So, each tissue class Ω_l is represented by the tuple $\langle \underline{A}(\Omega_l), \bar{A}(\Omega_l) \rangle$. According to the definitions of lower approximation and boundary region of rough sets [40], if a pixel $i \in \underline{A}(\Omega_l)$, then $i \notin B(\Omega_l), \forall l \in \mathcal{L}$, which signifies the pixel i is contained in Ω_l definitely. Integrating the concept of rough sets into the St- t distribution, the crisp lower approximation and probabilistic boundary region of Ω_l are defined as follows:

$$\underline{A}(\Omega_l) = \left\{ i \in \mathcal{S} : \left| \frac{\sqrt{u_i}(y_i - \beta_i - \mu_l)}{\sigma_l} \right| < k_l \right\}; \quad (9)$$

$$B(\Omega_l) = \left\{ i \in \mathcal{S} : i \notin \underline{A}(\Omega_p), \forall p \in \mathcal{L} \right\}. \quad (10)$$

The proposed simultaneous segmentation and bias field correction algorithm models the intensity distribution of the brain MR image as a mixture of finite number of St- t distributions and one uniform distribution. The uniform distribution is used to model the class Ω_{other} , which consists of CSF, pathologies, and other non-brain tissues and hence, has relatively large variance [17]. Accordingly, the brain MR image is represented as:

$$p(y_i | \beta_i) = \sum_{l: \Omega_l \sim \text{St-}t} p(y_i | \delta_{il}, \beta_i) p(\delta_{il} | x_{N_i}) + \lambda p(\Omega_{\text{other}}); \quad (11)$$

$$\text{where } p(y_i | \delta_{il}, \beta_i) = \int_{-\infty}^{\infty} p(y_i | u_i, \delta_{il}, \beta_i) p(u_i | \delta_{il}) du_i; \quad \Omega_l \sim \text{St-}t;$$

λ is the density of the uniform distribution, and $p(\delta_{il} | x_{N_i})$ denotes the probability that the i th pixel belongs to Ω_l , given the class labels of neighboring pixels N_i . In this regard, the joint EM-HMRF framework [50] is employed to incorporate spatial dependency into the proposed model. The neighborhood information of each pixel is incorporated into the proposed framework via the prior probability function $p(\delta_{il} | x_{N_i})$. The bias field

artifact $\underline{\beta} = (\beta_1, \beta_2, \dots, \beta_N)^T$ is modelled by an N -dimensional zero mean Gaussian prior probability density [46, 17, 50, 5]:

$$p(\underline{\beta}) = G'_{\psi_{\beta}}(\underline{\beta}); \quad \text{where } G'_{\psi_{\beta}}(\underline{x}) = \frac{1}{\sqrt{(2\pi)^N |\psi_{\beta}|}} \exp\left(-\frac{1}{2} \underline{x}^T \psi_{\beta}^{-1} \underline{x}\right).$$

3.2. The EM Algorithm

The objective of the EM algorithm is to find the MLE of parameters of the underlying distributions based on the observed incomplete data. To achieve this goal, a new set of latent variables is introduced in the problem that constitute the complete data together with the observed data. In proposed framework, the observed values of $y_i, i \in \mathcal{S}$ is the incomplete data, and the class labels x_i and latent variables u_i and $\delta_{il}, i \in \mathcal{S}, l \in \mathcal{L}$, together with $y_i, i \in \mathcal{S}$, constitute the complete data. To estimate the parameters, the Q -function, that is, the expected complete-data log-likelihood is constructed as:

$$\begin{aligned} Q(\theta | \theta^{(t)}) &= E[\log p(y, \underline{\beta}, \underline{x}, \underline{u} | x_{N_i}, \theta) | y, \theta^{(t)}] \\ &= \sum_{i \in \mathcal{S}} \sum_{l \in \mathcal{L}} \tau_{il}^{(t)} Q_{il}^{(t)} + \log p(\underline{\beta}), \end{aligned} \quad (12)$$

where $Q_{il}^{(t)} = E[\log p(y_i, x_i = l, u_i | \beta_i, x_{N_i}, \theta_l) | y_i, \theta_l^{(t)}]$ and $\tau_{il}^{(t)} = E[\delta_{il} | y_i, \beta_i, x_{N_i}, \theta_l^{(t)}]$. Now,

$$Q_{il}^{(t)} = \log p(l | x_{N_i}) + Q_{2,il}(\theta | \theta^{(t)}) + Q_{3,il}(\theta | \theta^{(t)}), \quad (13)$$

$$\begin{aligned} \text{where } Q_{2,il}(\theta | \theta^{(t)}) &= E[\log p(u_i | x_i = l, \theta_l) | y_i, \beta_i, \theta_l^{(t)}] \\ &= \left[\frac{\nu_l}{2} \log \left(\frac{\nu_l}{2} \right) - \log \Gamma \left(\frac{\nu_l}{2} \right) - \frac{\nu_l}{2} u_{il}^{(t)} + \left(\frac{\nu_l}{2} - 1 \right) (lu)_{il}^{(t)} \right], \end{aligned}$$

where $u_{il}^{(t)} = E[u_i|y_i, \beta_i, \theta_l^{(t)}]$ and $(lu)_{il}^{(t)} = E[\log u_i|y_i, \beta_i, \theta_l^{(t)}]$;

$$\begin{aligned} Q_{3,il}(\theta^{(t)}) &= E[\log p(y_i|u_i, \beta_i, x_i = l, \theta_l)|y_i, \theta_l^{(t)}] \\ &= \frac{1}{2}(lu)_{il}^{(t)} - \log D_l - \log \sigma_l - \frac{1}{2} \log(2\pi) - \frac{1}{2} E(z_{il}^2|y_i, \beta_i, \theta_l^{(t)}). \end{aligned}$$

$$\text{Here, } E(z_{il}^2|y_i, \beta_i, \theta_l^{(t)}) = \begin{cases} k_l^2, & \text{if } i \in \underline{A}(\Omega_l) \\ u_{il}^{(t)} \frac{(v_l - \beta_l - \mu_l)^2}{\sigma_l^2}, & \text{if } i \in \underline{B}(\Omega_l). \end{cases} \quad (14)$$

3.2.1. The Expectation (E)-Step

The posterior probability that the pixel i belongs to the tissue class Ω_l is given by

$$\begin{aligned} \tau_{il} &= E[\delta_{il}|y_i, \beta_i, x_{N_i}, \theta_l] = p(\delta_{il} = 1|y_i, \beta_i, x_{N_i}, \theta_l) \\ &= \frac{p(x_i = l|x_{N_i})p(y_i|x_i = l, \beta_i, \theta_l)}{\sum_{m \in \mathcal{L}} p(x_i = m|x_{N_i})p(y_i|x_i = m, \beta_i, \theta_m)}. \end{aligned} \quad (15)$$

So, the expression τ_{il} in (15) evidently computes the belongingness of pixel i to Ω_l , which can be considered as the membership value of pixel i to Ω_l . According to the definitions of lower approximation and boundary region of a tissue class, based on the St- t distribution and rough sets, if a pixel belongs to the lower approximation region of a specific tissue class, it should definitely belong to that tissue class. Hence, the membership of the pixel to that tissue class should be 1 and to other classes should be 0. On the other hand, the pixels in boundary regions should have different memberships to different classes as there exists ambiguity in its belongingness to a particular tissue class. So, the membership function is modified as

$$\tau_{il} = \begin{cases} 1, & \text{if } i \in \underline{A}(\Omega_l) \\ \frac{p(l|x_{N_i})p(y_i|l, \beta_i, \theta_l)}{\sum_{m \in \mathcal{L}} p(m|x_{N_i})p(y_i|m, \beta_i, \theta_m)}, & \text{else if } i \in \underline{B}(\Omega_l) \\ 0, & \text{otherwise.} \end{cases} \quad (16)$$

Since \underline{x} is considered as a realization of an MRF, its prior probability is derived from

$$p(\underline{x}) = \frac{1}{Z} \exp\{-E(\underline{x})\}, \quad (17)$$

Z being the normalizing constant, called the partition function, and $E(\underline{x})$ is an energy function of the form $E(\underline{x}) = \sum_{c \in \mathcal{C}} E_c(\underline{x})$,

which is a sum of clique potentials $E_c(\underline{x})$ over all possible cliques C . In this problem, we define the clique potential as $E_c(\underline{x}) = -a\delta(x_i - x_j)$, where a is the scale parameter. So,

$$p(x_i|x_{N_i}) = \frac{\exp\left(\sum_{j \in N_i} a\delta(x_i - x_j)\right)}{\sum_{m \in \mathcal{L}} \exp\left(\sum_{j \in N_i} s\delta(m - x_j)\right)} = \frac{\exp(an_i(x_i))}{\sum_{m \in \mathcal{L}} \exp(an_i(m))}, \quad (18)$$

where $n_i(x_i)$ is the number of neighbors of pixel i having class label x_i . Now, before estimating u_{il} and $(lu)_{il}$, the distribution of $U_{il}(Y_i = y_i, \delta_{il} = 1, \beta_i)$ is obtained as follows:

$$\begin{aligned} p(u_i|y_i, \delta_{il}, \beta_i) &= \frac{p(y_i|u_i, \delta_{il}, \beta_i)p(u_i|\delta_{il})}{p(y_i|\delta_{il}, \beta_i)} \\ &= \frac{1}{\Upsilon_{il}} \left(\frac{v_l}{2}\right)^{\frac{v_l+1}{2}} e^{-\frac{1}{2}(u_i v_l + z_{il}^2)} u_i^{\frac{v_l+1}{2}-1} I_{(0, \infty)}(u_i), \end{aligned} \quad (19)$$

where $\Upsilon_{il} = \left[e^{-\frac{k_l^2}{2}} \gamma\left(\frac{v_l+1}{2}, \frac{u_{0,il} v_l}{2}\right) + \frac{\Gamma\left(\frac{v_l+1}{2}, \frac{u_{0,il} v_l \zeta_{il}}{2}\right)}{\zeta_{il}^{\frac{v_l+1}{2}}}\right]$, $u_{0,il} = \frac{k_l^2}{d(y_i, \beta_i, \mu_i, \sigma_i)}$, and $\zeta_{il} = \left(1 + \frac{k_l^2}{u_{0,il} v_l}\right)$.

$$\begin{aligned} u_{il} &= E[u_i|y_i, \beta_i, \theta_l] = \int_{-\infty}^{\infty} u_i p(u_i|y_i, \delta_{il}, \beta_i) du_i \\ &= \frac{1}{\Upsilon_{il}} \frac{1}{\left(\frac{v_l}{2}\right)} \left[e^{-\frac{k_l^2}{2}} \gamma\left(\frac{v_l+3}{2}, \frac{u_{0,il} v_l}{2}\right) + \frac{\Gamma\left(\frac{v_l+3}{2}, \frac{u_{0,il} v_l \zeta_{il}}{2}\right)}{\zeta_{il}^{\frac{v_l+3}{2}}}\right]. \end{aligned} \quad (20)$$

$$\begin{aligned} (lu)_{il} &= E[\log u_i|y_i, \beta_i, \theta_l] = \int_{-\infty}^{\infty} \log u_i p(u_i|y_i, \delta_{il}, \beta_i) du_i \\ &= -\log\left(\frac{v_l}{2}\right) + \frac{1}{\Upsilon_{il}} \left[e^{-\frac{k_l^2}{2}} \int_0^{\frac{u_{0,il} v_l}{2}} e^{-t} t^{\frac{v_l-1}{2}} \log t dt \right. \\ &\quad \left. + \frac{\int_{\frac{u_{0,il} v_l \zeta_{il}}{2}}^{\infty} e^{-t} t^{\frac{v_l-1}{2}} \log t dt}{\zeta_{il}^{\frac{v_l+1}{2}}} - \log(\zeta_{il}) \frac{\Gamma\left(\frac{v_l+1}{2}, \frac{u_{0,il} v_l \zeta_{il}}{2}\right)}{\zeta_{il}^{\frac{v_l+1}{2}}}\right]. \end{aligned} \quad (21)$$

Further algebraic calculations lead to:

$$\begin{aligned} \int_0^{\frac{u_{0,il} v_l}{2}} e^{-t} t^{\frac{v_l-1}{2}} \log t dt &= \gamma'\left(\frac{v_l+1}{2}, \frac{u_{0,il} v_l}{2}\right) - e^{-\frac{u_{0,il} v_l}{2}} u_{0,il}^{\frac{v_l+1}{2}} \left(\frac{v_l}{2}\right)^{\frac{v_l-1}{2}} \\ \int_{\frac{u_{0,il} v_l \zeta_{il}}{2}}^{\infty} e^{-t} t^{\frac{v_l-1}{2}} \log t dt &= \Gamma'\left(\frac{v_l+1}{2}, \frac{u_{0,il} v_l \zeta_{il}}{2}\right) + e^{-\frac{u_{0,il} v_l \zeta_{il}}{2}} u_{0,il}^{\frac{v_l+1}{2}} \left(\frac{v_l \zeta_{il}}{2}\right)^{\frac{v_l-1}{2}} \end{aligned}$$

where $\gamma'(p, x) = \frac{\partial}{\partial p} \gamma(p, x)$ and $\Gamma'(p, x) = \frac{\partial}{\partial p} \Gamma(p, x)$.

The optimal labeling can be estimated according to the maximum a posteriori criterion

$$\begin{aligned} \hat{\underline{x}} &= \arg \max_{\underline{x}} [p(\underline{y}|\underline{x}, \underline{\beta})p(\underline{x})] \\ &= \arg \min_{\underline{x}} \left[-\sum_{i \in \mathcal{S}} \left(\log \Upsilon_{i, x_i} - \log D_{x_i} - \log \sigma_{x_i} \right. \right. \\ &\quad \left. \left. - \frac{1}{2} \log(\pi v_{x_i}) - \log \Gamma\left(\frac{v_{x_i}}{2}\right) \right) + E(\underline{x}) \right]. \end{aligned} \quad (22)$$

Using iterated conditional modes algorithm [9], this optimization problem is reduced to

$$\begin{aligned} \hat{x}_i &= \arg \min_{x_i} \left[\log D_{x_i} + \log \sigma_{x_i} + \frac{1}{2} \log(\pi v_{x_i}) \right. \\ &\quad \left. + \log \Gamma\left(\frac{v_{x_i}}{2}\right) - \log \Upsilon_{i, x_i} - an_i(x_i) \right]. \end{aligned} \quad (23)$$

3.2.2. The Maximization (M)-Step

Optimizing Q -function with respect to bias field β_i , we get:

$$\frac{\partial}{\partial \beta_i} \overline{R}_i^{(t)} - \overline{\psi}_{ii}^{-1(t)} \beta_i + \frac{\frac{\partial}{\partial \beta_i} p(\underline{\beta})}{p(\underline{\beta})} = 0, \quad (24)$$

where $\overline{R}_i^{(t)} = \sum_{l \in \mathcal{L}} \tau_{il}^{(t)} u_{il}^{(t)} \frac{(y_i - \mu_l)}{\sigma_l^2}$ is the mean residual and the mean inverse covariance is

$$\overline{\psi}^{-1}_{ip} = \begin{cases} \sum_{l \in \mathcal{L}} \tau_{il}^{(t)} u_{il}^{(t)} \frac{1}{\sigma_l^2}, & \text{if } i = p \\ 0, & \text{otherwise.} \end{cases} \quad (25)$$

Further operations on (24) lead to

$$\underline{\hat{\beta}}^{(t+1)} = H \overline{R}^{(t)}, \quad (26)$$

where $H = [\overline{\psi}^{-1} + \psi_{\beta}^{-1}]^{-1}$. Since, estimating ψ_{β} , and hence ψ_{β}^{-1} , is computationally infeasible, H is estimated using a linear low-pass filter [46]. So, the bias field at i th pixel is estimated as

$$\hat{\beta}_i^{(t+1)} = \frac{[F \overline{R}^{(t)}]_i}{[F \overline{\psi}^{-1}]_i}, \quad (27)$$

where F is a low-pass filter. Optimizing Q with respect to parameters μ_l and σ_l , we get:

$$\hat{\mu}_l^{(t+1)} = \frac{\sum_{i \in B(\Omega_l)} \tau_{il}^{(t)} u_{il}^{(t)} (y_i - \beta_i)}{\sum_{i \in B(\Omega_l)} \tau_{il}^{(t)} u_{il}^{(t)}}, \quad (28)$$

$$\text{and } (\hat{\sigma}_l^2)^{(t+1)} = \frac{\sum_{i \in B(\Omega_l)} \tau_{il}^{(t)} u_{il}^{(t)} (y_i - \beta_i - \hat{\mu}_l^{(t+1)})^2}{\sum_{i \in S} \tau_{il}^{(t)}}. \quad (29)$$

Following [24], the denominator $\sum_{i \in S} \tau_{il}^{(t)}$ in (29) is replaced by $\sum_{i \in S} \tau_{il}^{(t)} u_{il}^{(t)}$ for faster convergence of the EM algorithm. Hence, the estimate of $(\hat{\sigma}_l^2)^{(t+1)}$ is modified to:

$$(\hat{\sigma}_l^2)^{(t+1)} = \frac{\sum_{i \in B(\Omega_l)} \tau_{il}^{(t)} u_{il}^{(t)} (y_i - \beta_i - \hat{\mu}_l^{(t+1)})^2}{\sum_{i \in S} \tau_{il}^{(t)} u_{il}^{(t)}}. \quad (30)$$

However, the removal of lower approximation region from parameter estimation in (28) and (30) creates estimation bias, since it assigns higher weightage in the boundary region, which in presence of noise and outliers degrades the parameter estimation. The derived estimate of μ_l in (28) considers only bias corrected intensity in the boundary region, not lower approximation region. Hence, $\hat{\mu}_l$ is modified to incorporate the effects of both lower approximation and boundary region, as follows:

$$\hat{\mu}_l^{(t+1)} = \frac{\sum_{i \in \underline{A}(\Omega_l)} u_{il}^{(t)} (y_i - \beta_i) + \sum_{i \in B(\Omega_l)} \tau_{il}^{(t)} u_{il}^{(t)} (y_i - \beta_i)}{\sum_{i \in \underline{A}(\Omega_l)} u_{il}^{(t)} + \sum_{i \in B(\Omega_l)} \tau_{il}^{(t)} u_{il}^{(t)}}. \quad (31)$$

Similarly, in the estimate of σ_l^2 , the weighted squared deviation of intensity values from their mean in lower approximation region is included in the numerator, as follows:

$$(\hat{\sigma}_l^2)^{(t+1)} = \frac{\sum_{i \in \underline{A}(\Omega_l)} u_{il}^{(t)} (y_i - \beta_i - \hat{\mu}_l^{(t+1)})^2 + \sum_{i \in B(\Omega_l)} \tau_{il}^{(t)} u_{il}^{(t)} (y_i - \beta_i - \hat{\mu}_l^{(t+1)})^2}{\sum_{i \in \underline{A}(\Omega_l)} u_{il}^{(t)} + \sum_{i \in B(\Omega_l)} \tau_{il}^{(t)} u_{il}^{(t)}}. \quad (32)$$

The variable u_{il} estimates the inlierness of the i th pixel to Ω_l . If the pixel lies very near to the cluster centroid (class mean), the corresponding value of u will be very high, while an outlier pixel will produce negligible (near to zero) value of u . Thus, introducing the novel variable u , the proposed t -StoRM algorithm filters out the effects of outlier pixels from the estimate of the parameters, which pose a serious threat during any moment-based parameter estimation. Additionally, the variable u assigns higher weightage to the pixels belonging in lower approximation region, which enables the t -StoRM to provide robust parameter estimation even in heavy noisy environment. The StoRM algorithm [5] also performs similar kind of operation during parameter estimation; but instead of estimating the weight adaptively, it assigns constant (higher) weight to the pixels in lower approximation region and constant (lower) weight to the pixels in boundary region (containing noise and outliers). The introduction of u in t -StoRM nullifies the need of this pre-specified fixed weight and provides efficient computation of the individual contributions of inlier and outlier pixels, thus producing robust estimates of parameters.

The estimates of the parameters k_l and ν_l are obtained using the approach mentioned in [7]. Optimizing Q with respect to k_l and applying the numerical Newton-Raphson method, the estimate of k_l is obtained as follows: start with an initial estimate of k_l , that is, $(k_l)_0$. The process is repeated as

$$(k_l)_{n+1} = (k_l)_n - \frac{f((k_l)_n)}{f'((k_l)_n)}, \quad (33)$$

until it converges to an optimum solution, where

$$f(k) = (1 - \Phi(k)) \sum_{i \in \underline{A}(\Omega_l)} \tau_{il}^{(t)} - k \phi(k) \sum_{i \in B(\Omega_l)} \tau_{il}^{(t)} \quad (34)$$

$$\text{and } f'(k) = \phi(k) \left[k^2 \sum_{i \in B(\Omega_l)} \tau_{il}^{(t)} - \sum_{i \in S} \tau_{il}^{(t)} \right]. \quad (35)$$

In the similar way, the estimate of ν_l is obtained as: start with an initial estimate of ν_l , that is, $(\nu_l)_0$. The process is repeated as

$$(\nu_l)_{n+1} = (\nu_l)_n - \frac{g((\nu_l)_n)}{g'((\nu_l)_n)}, \quad (36)$$

until it converges to an optimum solution, where

$$g(k) = 1 + \log\left(\frac{k}{2}\right) - \psi\left(\frac{k}{2}\right) + \frac{1}{\tau_l^{(t)}} \sum_{i \in S} \tau_{il}^{(t)} ((lu)_{il}^{(t)} - u_{il}^{(t)}),$$

$$g'(k) = \frac{1}{k} - \frac{1}{2} \psi'\left(\frac{k}{2}\right), \quad \tau_l^{(t)} = \sum_{i \in S} \tau_{il}^{(t)}, \quad \psi(p) = \frac{1}{\Gamma(p)} \frac{\partial}{\partial p} \Gamma(p)$$

is the digamma function, and $\psi'(p) = \frac{\partial}{\partial p} \psi(p)$ is the trigamma function. The algorithm of the proposed t -StoRM method is presented in Algorithm 1.

Complexity Analysis. For each iteration of the t -StoRM algorithm, the estimation of memberships takes $O(RCL)$ time, where the image is of size $R \times C$ and the number of tissue classes is L . Estimation of u , lu , and class labels are all performed in $O(RCL)$ time; while the estimation of bias field components

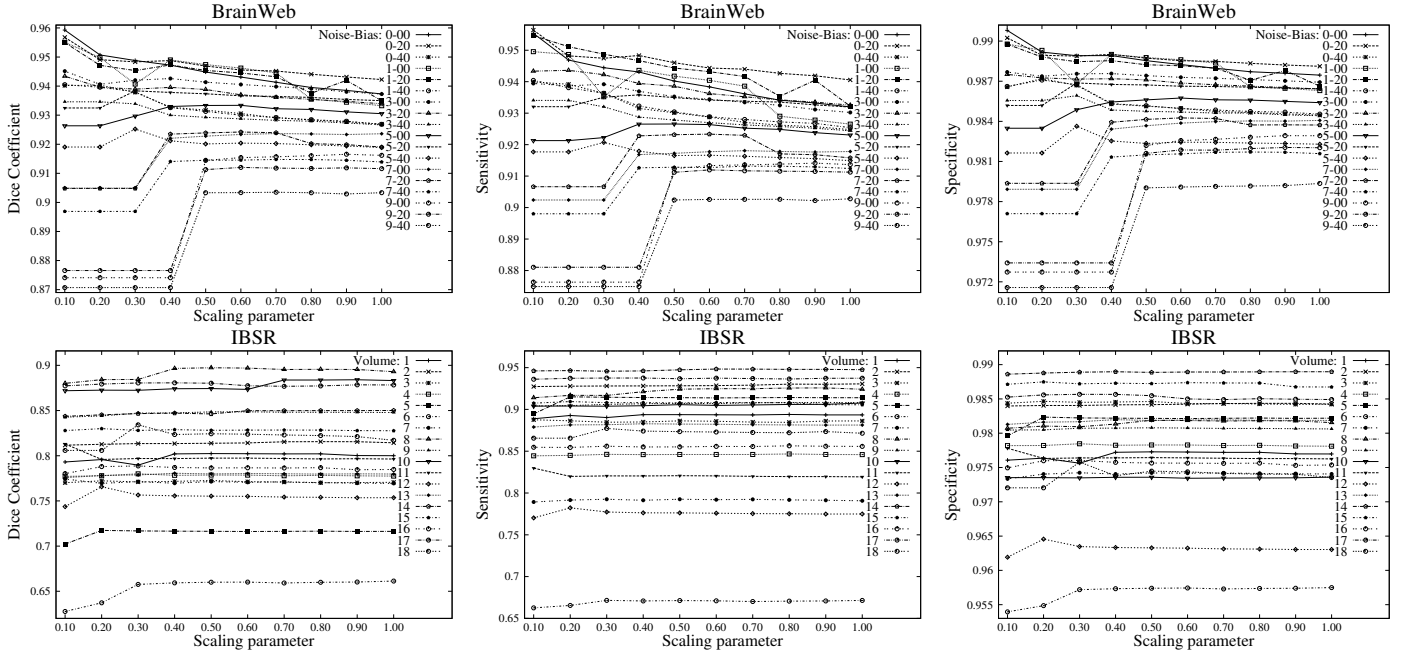


Figure 4. Variation of scaling parameter a in t -StoRM with respect to different segmentation evaluation indices.

Algorithm 1: t -StoRM for Simultaneous Segmentation and Bias Field Correction

Input : Input image, number of tissue classes.

Output: Segmented and bias field corrected images.

- 1 Initial segmentation and parameter estimation;
 - 2 **do**
 - 3 Estimate the membership values using (16);
 - 4 Estimate u and lu using (20) and (21), respectively;
 - 5 Estimate the class labels using (23);
 - 6 Estimate the logarithm of bias field using (27);
 - 7 Update parameters μ_l and σ_l^2 using (31) and (32), respectively;
 - 8 Update the width parameter k_l using (33);
 - 9 Update ν_l using (36);
 - 10 $t \leftarrow t + 1$;
 - 11 **while** the algorithm does not converge and the maximum number of iterations has not reached;
 - 12 Construct the segmented and bias field corrected images.
-

takes $O(RCL\Delta^2)$ time, where Δ is the maximum window size of the low-pass filter. Updation of parameters μ_l and σ_l^2 are also performed in $O(RCL)$ time. Updating parameters k_l and ν_l takes, respectively, $O(RCLT'_1)$ and $O(RCLT'_2)$ time, where T'_1 and T'_2 are the number of iterations to converge the numerical methods. In practice, $T'_1, T'_2 \leq 10$. So, for T iterations, the time complexity of the proposed t -StoRM algorithm is $O(RCLT(\Delta^2 + T'_1 + T'_2)) = O(RCLT\Delta^2)$, as $\Delta^2 > T'_1 + T'_2$.

Generalization of Existing Algorithms. The proposed t -StoRM algorithm is the generalization of some of the existing simultaneous segmentation and bias field correction algorithms. In case $\nu_l \rightarrow \infty$, $\forall l \in \mathcal{L}$, the St- t distribution reduces to StN dis-

tribution. In turn, the proposed algorithm reduces to the StoRM algorithm [5]. If $\nu_l \rightarrow \infty$ and $k_l = 0$, $\forall l \in \mathcal{L}$, the St- t distribution reduces to normal distribution. In this case, the image is represented by a finite mixture of normal distributions. Hence, the proposed algorithm reduces to the HMRF-EM algorithm [50]. On the other hand, if the parameters of St- t distributions are neither estimated through the HMRF nor updated in each iteration, but estimated previously before applying the algorithm, the proposed algorithm reduces to the modified EM (mEM) algorithm [17] for $k_l = 0$ and $\nu_l \rightarrow \infty$. Moreover, if the class Ω_{other} is modelled using St- t distribution with $k_l = 0$ and $\nu_l \rightarrow \infty$, instead of uniform distribution, t -StoRM reduces to the adaptive segmentation (ASeg) algorithm [46].

4. Experimental Results and Discussion

The performance of the proposed t -StoRM algorithm, based on St- t distribution, rough sets, and HMRF model, is studied and compared with that of several existing simultaneous segmentation and bias field correction algorithms, namely, ASeg [46], mEM [17], HMRF-EM [50], MICO [28], StN distribution, rough sets, and HMRF model based simultaneous segmentation and bias field correction algorithm (StoRM) [5], Student's- t distribution and EM algorithm based simultaneous segmentation and bias field correction algorithm (t EM) [8], and bias-corrected FCM algorithm (BCFCM); existing bias field correction algorithms, namely, rough sets and contraharmonic mean filter based bias field correction method (RC2) [4] and non-parametric nonuniform intensity normalization bias correction method (N3) [44]; several brain MR image segmentation algorithms: kernel metric and trade-off weighted fuzzy factor based fuzzy local information c -means (KWFLICM) [16], RFCM [32, 33, 34], rRFCM [37, 36], deviation-sparse FCM with neighbor information constraint (DSFCM-N) [49], intuitionistic center-

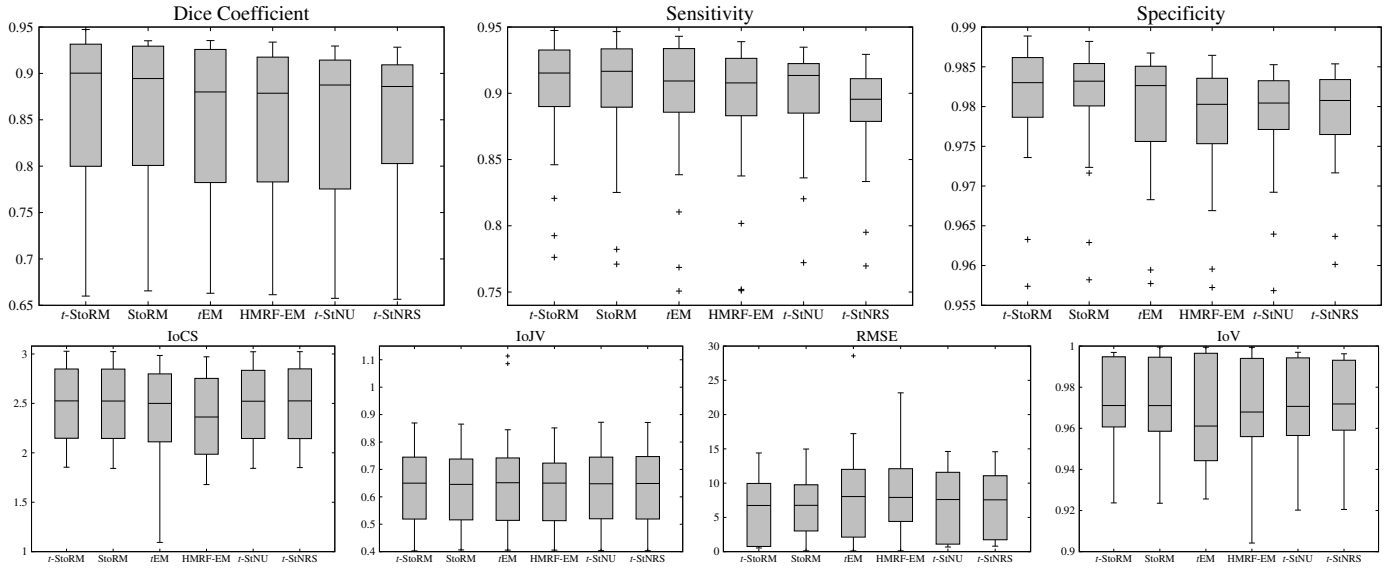


Figure 5. Box plot depicting the importance of proposed t -StoRM framework with respect to segmentation and bias field correction evaluation indices.

free FCM (ICFFCM) [3], and improved FCM based on morphological reconstruction and membership filtering (FRFCM) [27]; and several analysis tools for MRI, namely, statistical parameter mapping software (SPM) version 8 [2] and FMRIB Software Library (FSL) version 5.0 [20]. Before applying the algorithms on brain MR images, the brain extraction tool [45] is applied to remove non-brain tissues like skull, scalp, dura, etc., from the images; while the thresholding method due to Otsu [39] is applied for initial segmentation of the brain MR images and to estimate the initial set of parameters of different brain tissue classes. The proposed t -StoRM algorithm, ASeg, mEM, HMRF-EM, StoRM, and RC2 algorithms are implemented in C language. All the algorithms and measures are executed in Ubuntu 16.04 LTS 64-bit OS having machine configuration Intel(R) Core(TM) i7-2600 CPU @3.40GHz \times 8 and 16 GB RAM. The source code of the proposed t -StoRM algorithm is available at: www.isical.ac.in/~bibl/results/t-storm.html.

To analyze the performance of different algorithms, the experimentation is done on some benchmark simulated MR images of “BrainWeb: Simulated Brain Database”² [11, 25, 12] and real MR images of “IBSR: Internet Brain Segmentation Repository”³. The brain MR images of BrainWeb database are generated using an MRI simulator by varying different noise levels (0%, 1%, 3%, 5%, 7%, and 9%) and intensity inhomogeneity artifacts (0%, 20%, and 40%) present in the image. The anatomical model serves as the ground truth segmentation of the generated volumes. The “percent noise” number represents the percent ratio of the standard deviation of the additive white Gaussian noise versus the signal for the brightest tissue. From IBSR database, all eighteen volumes (volumes 1 to 18) are used in the current study. For each volume of IBSR database, the manual segmentation by an expert supervisor is provided, which serves as the gold standard for segmentation. All the image volumes of BrainWeb and IBSR are of size $181 \times 217 \times 181$

Table 1. Average p-Values of Proposed t -StoRM Algorithm for Different Values of Scaling Parameter

Scale (a)	Dice	Sensitivity	Specificity
0.10	0.918164	0.814450	0.959242
0.20	0.891274	0.725203	0.870370
0.30	0.767295	0.797424	0.762463
0.40	0.555834	0.544265	0.608914
0.50	0.029867	0.019692	0.023249
0.60	0.160750	0.140769	0.111611
0.70	0.194282	0.272680	0.241223
0.80	0.368789	0.450396	0.359192
0.90	0.482030	0.523890	0.467599
1.00	0.631713	0.711231	0.596136

and $256 \times 128 \times 256$, respectively. The middle slice of each volume is considered for both qualitative and quantitative analysis.

The performance of different bias field correction algorithms is evaluated using four quantitative indices, namely, index of class separability (IoCS) [4], index of joint variation (IoJV) [4], root mean square error (RMSE), and index of variation (IoV) [4]. A good bias correction method should make the values of IoCS and IoV as high as possible and that of IoJV and RMSE as low as possible. Since the ground truth or bias-free images are not available for the volumes of IBSR database, the restored images of IBSR database are compared with respect to only IoCS and IoJV. The performance of different segmentation algorithms is evaluated using three quantitative indices, namely, Dice coefficient, sensitivity, and specificity. The metrics are calculated for individual tissues (CSF, GM, and WM) and then averaged over all classes, indicating that the identification of all classes is given equal importance towards the calculation of segmentation accuracy. A good segmentation algorithm should make the values of these three indices as high as possible, and ideally, the values should be equal to 1. The bias field correction and segmentation evaluation indices computed over all brain MR images of BrainWeb and IBSR databases are graph-

²<http://www.bic.mni.mcgill.ca/brainweb/>

³<http://www.cma.mgh.harvard.edu/ibsr/>

Table 2. Estimated Parameters of St-t Distribution for Brain MR Images of BrainWeb and IBSR Databases

Vol. No.	GM				WM			
	μ_l	σ_l	k_l	ν_l	μ_l	σ_l	k_l	ν_l
0-0	4.700	0.107	0.130	2.109	4.999	0.029	0.028	5.504
0-20	4.647	0.110	0.108	3.002	4.951	0.041	0.070	5.368
0-40	4.595	0.115	0.132	3.026	4.903	0.053	0.091	5.663
1-0	4.683	0.103	0.143	3.022	4.982	0.035	0.064	5.248
1-20	4.644	0.110	0.104	3.005	4.947	0.041	0.063	5.460
1-40	4.588	0.116	0.088	3.004	4.897	0.054	0.091	5.695
3-0	4.620	0.107	0.108	3.041	4.917	0.043	0.079	5.467
3-20	4.591	0.113	0.102	3.006	4.894	0.048	0.068	5.574
3-40	4.560	0.122	0.082	3.025	4.872	0.058	0.108	6.696
5-0	4.572	0.120	0.087	3.027	4.874	0.057	0.123	5.598
5-20	4.546	0.126	0.089	3.009	4.854	0.059	0.060	5.458
5-40	4.515	0.130	0.081	3.091	4.828	0.067	0.099	5.694
7-0	4.542	0.139	0.104	3.033	4.851	0.070	0.099	5.215
7-20	4.551	0.135	0.076	2.984	4.863	0.072	0.047	5.571
7-40	4.492	0.144	0.067	3.320	4.809	0.074	0.100	5.573
9-0	4.496	0.154	0.097	2.988	4.815	0.081	0.090	5.222
9-20	4.506	0.152	0.067	2.988	4.826	0.082	0.081	5.433
9-40	4.465	0.154	0.097	3.065	4.786	0.083	0.090	5.457
V1	4.299	0.118	0.042	3.130	4.570	0.054	0.064	5.664
V2	4.252	0.112	0.093	3.630	4.513	0.047	0.074	5.912
V3	3.723	0.123	0.112	3.873	4.052	0.073	0.138	5.769
V4	3.849	0.125	0.157	3.803	4.197	0.075	0.066	5.719
V5	4.290	0.112	0.051	3.382	4.581	0.044	0.102	5.730
V6	4.054	0.121	0.051	2.902	4.306	0.034	0.000	4.875
V7	3.540	0.206	0.060	3.301	4.049	0.061	0.146	5.498
V8	3.582	0.274	0.023	5.173	4.135	0.065	0.000	6.014
V9	3.785	0.209	0.091	3.742	4.278	0.064	0.092	5.522
V10	3.493	0.240	0.106	3.629	4.057	0.065	0.125	5.335
V11	4.217	0.185	0.050	3.391	4.666	0.058	0.081	5.477
V12	3.585	0.203	0.052	3.204	4.054	0.076	0.096	5.664
V13	3.863	0.111	0.123	3.736	4.177	0.074	0.000	5.633
V14	3.707	0.125	0.056	3.765	4.079	0.058	0.000	5.552
V15	3.699	0.117	0.094	4.164	4.046	0.054	0.000	5.532
V16	3.802	0.120	0.096	4.016	4.183	0.081	0.072	5.814
V17	3.825	0.114	0.049	3.686	4.125	0.068	0.099	5.721
V18	3.928	0.161	0.060	3.229	4.355	0.077	0.026	5.800

ically presented using box-and-whisker plot. The significance analysis of the bias field correction and segmentation results is performed with the help of Wilcoxon signed-rank test and paired *t*-test (both one-tailed), with 0.05 as the level of significance. The bias field corrected and segmented images are also compared using intensity histograms.

4.1. Estimation of Scaling Parameter

The scaling parameter *a* in (23) is an important parameter, as it controls the overall segmentation performance of the *t*-StoRM algorithm. The parameter assigns weights to the clique potentials of the class label distribution, which, in turn, regulates the balance between the intensity and spatial connectedness of each pixel and provides optimal segmentation.

To obtain the optimal value of the scaling parameter, the parameter *a* is varied from 0.10 to 1.0 with common difference 0.10, and the performance of *t*-StoRM is studied with respect to Dice coefficient, sensitivity, and specificity. The value of 0.10 of the scaling parameter *a* indicates higher weightage on the intensity information and lower weightage on the connectedness property; while the value of 1.0 indicates higher weightage on the connectedness property. The value 0.0 of *a* actually nullifies

Table 3. Statistical Significance Analysis of Proposed *t*-StoRM Framework with respect to Segmentation and Bias Field Correction Evaluation Indices

Algorithm	Mean	Std. Dev.	p-value	
			Wilcoxon	Paired <i>t</i>
Dice Coefficient				
<i>t</i> -StoRM	0.865869	0.077326	-	-
StoRM	0.863866	0.073919	0.0808	0.0810
<i>t</i> EM	0.850978	0.080874	8.0E-10	1.4E-08
HMRf-EM	0.846023	0.079459	2.0E-09	2.6E-08
<i>t</i> -StNU	0.847821	0.080372	2.5E-08	1.0E-07
<i>t</i> -StNRS	0.853573	0.068812	6.5E-07	8.6E-05
Sensitivity				
<i>t</i> -StoRM	0.898918	0.056861	-	-
StoRM	0.898724	0.055875	0.3290	0.4227
<i>t</i> EM	0.893436	0.059085	5.5E-03	2.1E-03
HMRf-EM	0.889393	0.058645	1.4E-03	3.6E-04
<i>t</i> -StNU	0.888063	0.059069	2.8E-05	2.4E-05
<i>t</i> -StNRS	0.883008	0.048152	5.8E-07	1.0E-05
Specificity				
<i>t</i> -StoRM	0.981619	0.006873	-	-
StoRM	0.981145	0.006402	0.0496	0.0370
<i>t</i> EM	0.979605	0.007296	2.4E-07	8.2E-08
HMRf-EM	0.978343	0.007022	1.3E-07	1.1E-06
<i>t</i> -StNU	0.978221	0.007402	1.8E-08	9.7E-08
<i>t</i> -StNRS	0.979236	0.005556	1.2E-03	8.8E-04
IoCS				
<i>t</i> -StoRM	2.459574	0.472441	-	-
StoRM	2.454317	0.469986	4.9E-03	0.0243
<i>t</i> EM	2.318241	0.622233	2.3E-06	5.8E-03
HMRf-EM	2.274353	0.581766	1.5E-10	9.9E-05
<i>t</i> -StNU	2.450659	0.469502	1.1E-03	9.4E-04
<i>t</i> -StNRS	2.452097	0.469140	0.0173	7.9E-03
IoJV				
<i>t</i> -StoRM	0.654734	0.233891	-	-
StoRM	0.653173	0.233154	0.8888	0.9520
<i>t</i> EM	0.693854	0.298418	0.6248	0.0751
HMRf-EM	0.684957	0.296624	0.1812	0.1366
<i>t</i> -StNU	0.656612	0.234347	0.0125	0.0129
<i>t</i> -StNRS	0.656680	0.234529	0.0100	0.0108
RMSE				
<i>t</i> -StoRM	6.421026	5.037745	-	-
StoRM	6.722482	4.826283	0.1964	0.0910
<i>t</i> EM	8.225153	7.314029	0.3047	0.1313
HMRf-EM	12.357423	19.785690	0.1733	0.1170
<i>t</i> -StNU	7.085362	5.117368	5.3E-05	6.6E-04
<i>t</i> -StNRS	7.172256	4.866223	7.2E-05	5.1E-05
IoV				
<i>t</i> -StoRM	0.969831	0.023606	-	-
StoRM	0.970510	0.023960	0.7101	0.8083
<i>t</i> EM	0.965740	0.024741	0.5000	0.1352
HMRf-EM	0.966463	0.026426	0.8267	0.2683
<i>t</i> -StNU	0.968229	0.025020	0.0171	9.1E-03
<i>t</i> -StNRS	0.969005	0.023967	0.0269	0.0499

the connectedness property (HMRf model) and assumes that the pixels are spatially independent. The effect of the scaling parameter *a* in the *t*-StoRM algorithm is presented in Figure 4 with respect to Dice coefficient, sensitivity, and specificity for all brain MR images of BrainWeb and IBSR databases.

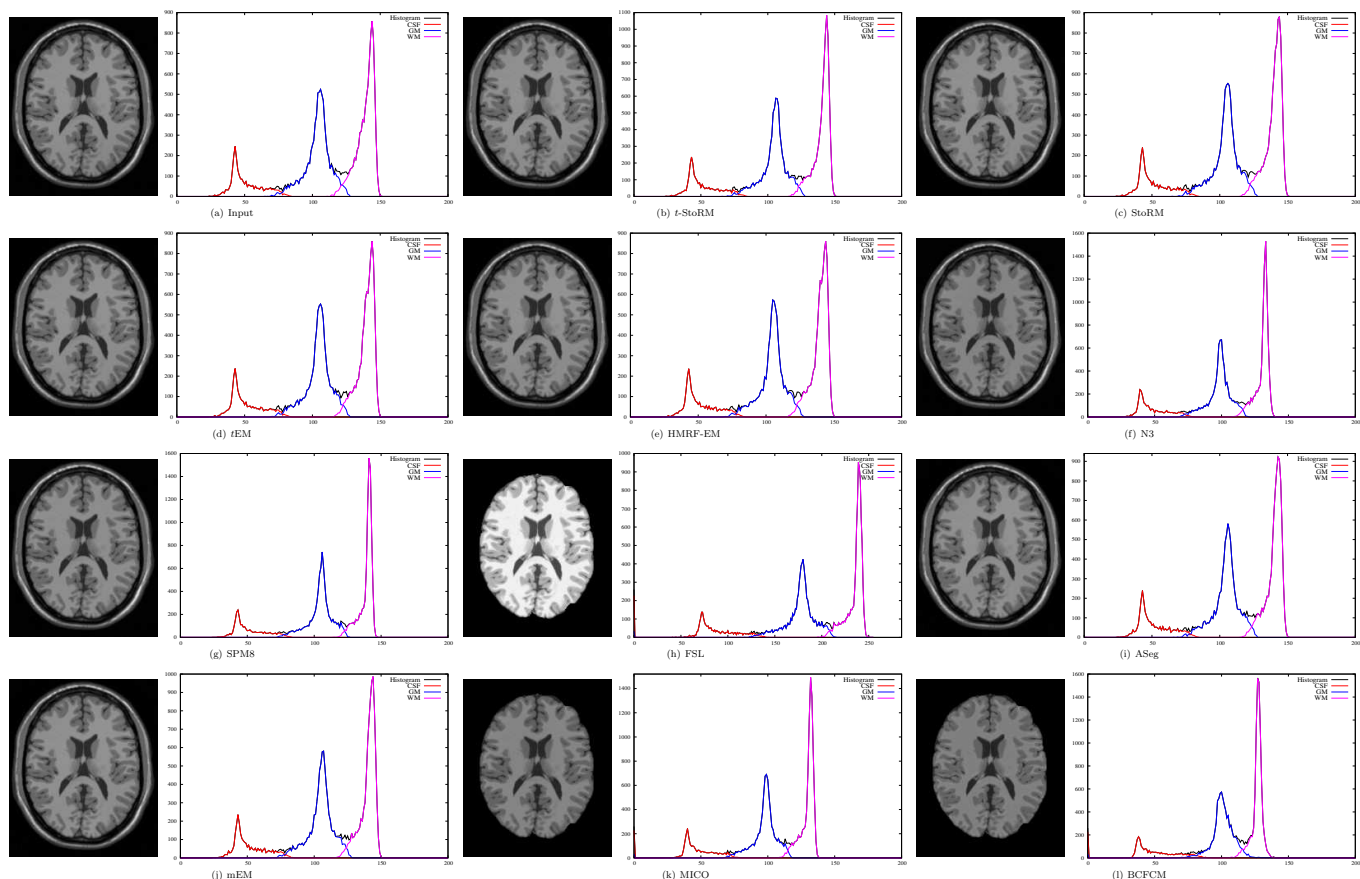


Figure 6. Input image of BrainWeb with 1% noise and 20% bias field and images restored by different algorithms, along with the intensity histograms.

To find the optimal scaling parameter a^* , a novel technique is incorporated that applies the method of statistical hypothesis testing. For each scaling parameter a and b , $a, b = 0.10, 0.20, \dots, 1.0, a \neq b$, the null hypothesis is defined as $H_{0,ab} : \mu_a = \mu_b$, implying the average performance of t -StoRM using scaling parameters a and b is same. The alternative hypothesis is defined as $H_{1,ab} : \mu_a > \mu_b$, implying the average performance of t -StoRM using scaling parameter a is better than that of using parameter b . The significance analysis of the paired t -test is evaluated using p-value, denoted by p_{ab} , with level of significance 0.05.

For each scaling parameter a , the p-values p_{ab} with respect to other scaling parameters $b = 0.10, 0.20, \dots, 1.0, b \neq a$, are calculated. The average p-value $p_a = \frac{1}{9} \sum_{b \neq a} p_{ab}$ indicates the average performance improvement using the scaling parameter a over other scaling parameters. The scaling parameter, which attains the minimum average p-value, should provide optimal segmentation performance, as it consistently provides better segmentation than using other scaling parameters. From the results presented in Table 1, it can be easily observed that the average performance of the proposed t -StoRM algorithm at $a = 0.50$ is not only better than that of other scaling parameters, but also significantly better, considering 0.05 as the level of significance, with respect to all segmentation evaluation indices. So, for further experimentation, the value of the scaling parameter a is fixed to 0.50, as that specific value of the parameter provides the optimal segmentation performance.

4.2. Parameter Estimation of Stopped- t Distribution

Table 2 reports the estimated parameters μ_l, σ_l, k_l , and ν_l for tissue classes GM and WM. The CSF, pathologies, and other non-brain tissues are unified together into Ω_{other} with uniform distribution, as the variance of these classes is very large [17]. The zero value of k_l implies that the algorithm applies Student's t -distribution, instead of St- t distribution, to represent the intensity distribution of the tissue class. From the results reported in Table 2, it can be easily observed that, for five images of IBSR database, the GM region is represented by St- t distribution, while the corresponding WM region is modelled using Student's t -distribution. In all other cases of BrainWeb and IBSR databases, both GM and WM regions are modelled using St- t distribution.

4.3. Importance of St- t Distribution

To establish the importance of St- t distribution over other distributions such as StN, Student's t , and Gaussian distributions for simultaneous segmentation and bias field correction in brain MR images, experimentation is carried out on several images. The StoRM algorithm [5] applies the finite mixture of StN distributions to model a brain MR image. So, by comparing the proposed t -StoRM algorithm with the StoRM algorithm, the comparison of the St- t distribution with StN distribution for brain MR image segmentation has been performed. Similarly, the HMRf-EM algorithm [50] models a brain tissue class using the unimodal Gaussian distribution in the joint EM-HMRf

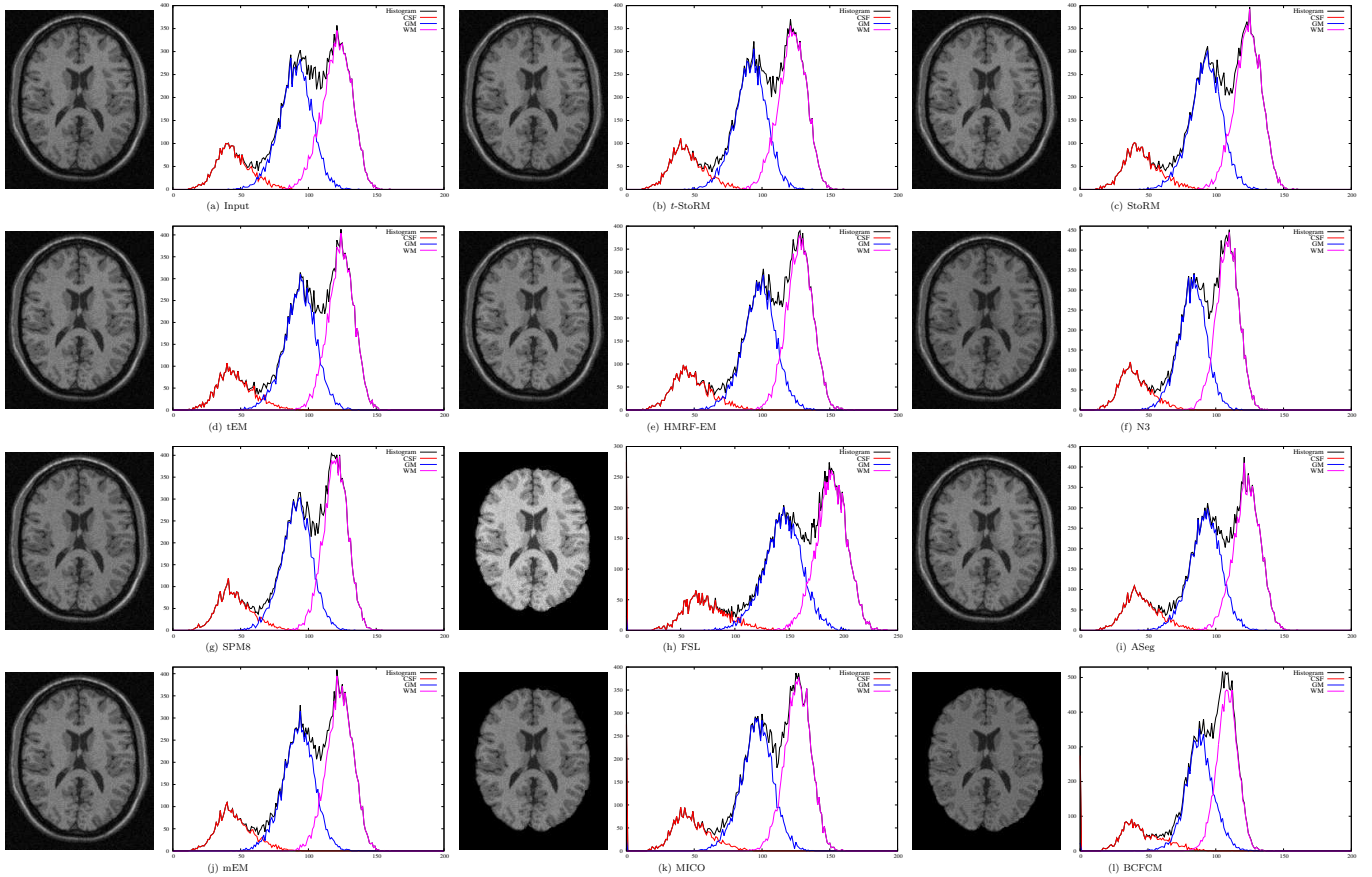


Figure 7. Input image of BrainWeb with 7% noise and 40% bias field and images restored by different algorithms, along with the intensity histograms.

framework. Hence, the importance of $St-t$ distribution over Gaussian distribution is demonstrated by comparing the performance of t -StoRM and HMRF-EM algorithms. Moreover, the importance of $St-t$ distribution over Student's t -distribution is demonstrated by comparing the performance of proposed algorithm with that of the t EM algorithm [8], which models each brain tissue class using Student's t -distribution for simultaneous segmentation and bias field correction. The comparative bias field correction and segmentation performance analysis is depicted in Figure 5 using box-and-whisker plot. The significance analysis is presented in Table 3 for the proposed t -StoRM, StoRM, t EM, and HMRF-EM algorithms with respect to different segmentation and bias field correction evaluation indices.

From the results reported in the top row of Figure 5 and top three blocks of Table 3 for segmentation evaluation, it is clear that the proposed t -StoRM achieves significantly better segmentation results compared to the t EM and HMRF-EM, irrespective of the quantitative indices and statistical tests used. The proposed algorithm also attains significantly better segmentation performance than the StoRM with respect to specificity, while better but not significant performance (marked in italics) with respect to both Dice coefficient and sensitivity.

From the results reported in the bottom row of Figure 5 and bottom four blocks of Table 3, it can be easily observed that the proposed t -StoRM algorithm provides significantly better restoration performance than StoRM, t EM, and HMRF-EM with respect to IoCS index, irrespective of the statistical tests

used. With respect to IoJV index, the performance of the proposed t -StoRM algorithm is better but not significant (marked in italics) than HMRF-EM algorithm; whereas the StoRM algorithm provides better restoration performance (marked in bold) than the t -StoRM. The proposed algorithm also attains better but not significant restoration performance than t EM with respect to IoJV, when compared in terms of p-values computed through paired t -test; while the performance of t EM is better, when compared using Wilcoxon signed-rank test. With respect to RMSE, the t -StoRM algorithm provides better but not significant restoration performance than the StoRM, t EM, and HMRF-EM, irrespective of the statistical tests used. With respect to IoV, the proposed t -StoRM achieves better but not significant restoration performance compared to t EM, while the StoRM achieves better but not significant restoration performance compared to t -StoRM. The t -StoRM algorithm also provides better but not significant restoration performance than HMRF-EM with respect to IoV, when compared using paired t -test; while the performance of HMRF-EM is better but not significant, when compared using Wilcoxon signed-rank test.

The qualitative analysis of the bias field correction performance of t -StoRM algorithm over StoRM, t EM, and HMRF-EM algorithms is presented in Figures 6, 7, 8, and 9. Similarly, the segmented images by t -StoRM, StoRM, t EM, and HMRF-EM algorithms are presented in Figures 11, 13, 15, and 16. The corresponding intensity histogram for each bias corrected and segmented image is also provided. All the results reported in

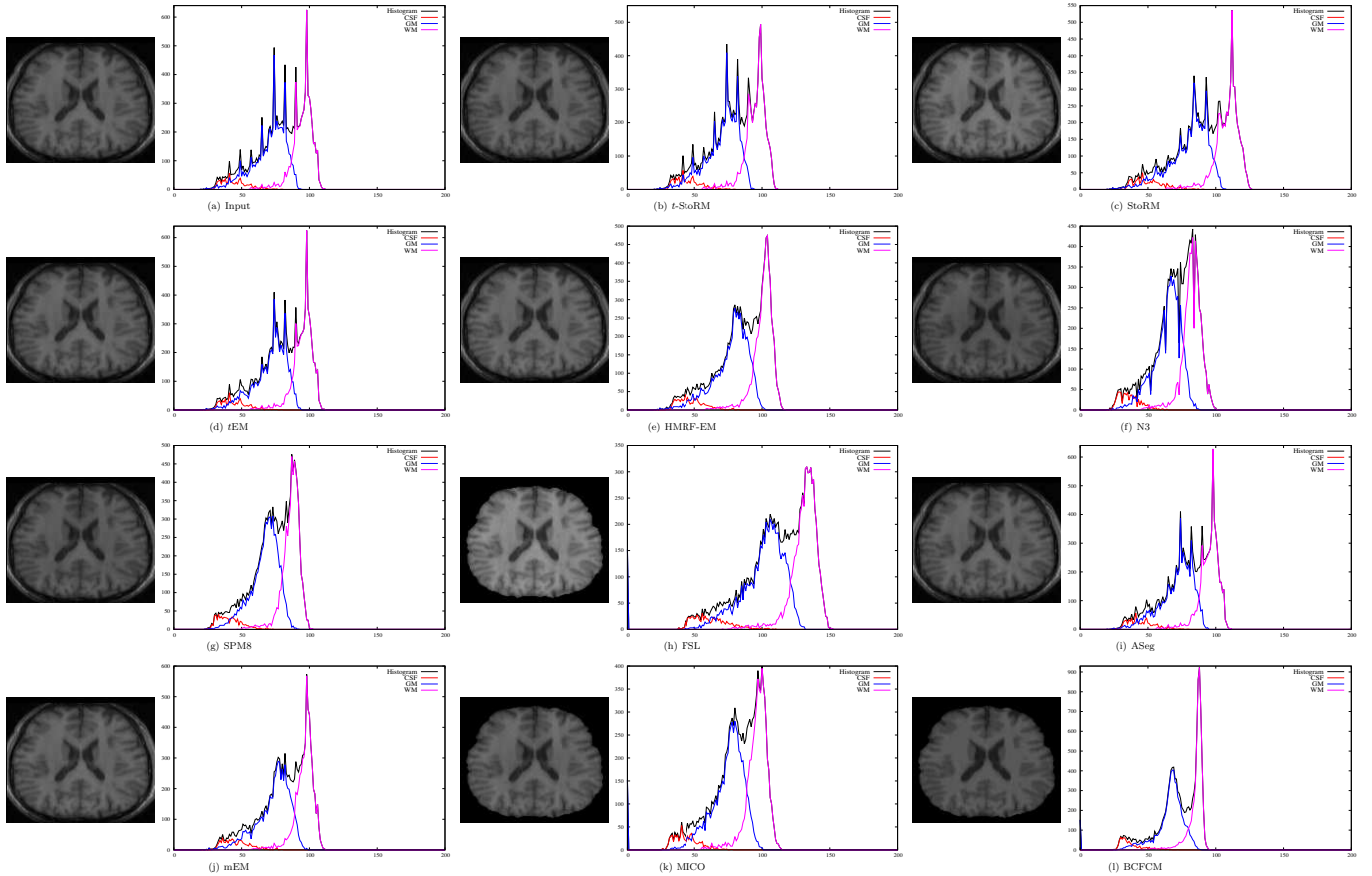


Figure 8. Input image of IBSR volume no. 1 and images restored by different algorithms, along with the intensity histograms.

these figures establish the importance of using $St-t$ distribution in terms of both bias field correction and segmentation.

4.4. Importance of Uniform Distribution for “Other” Class

To establish the importance of using uniform distribution to model the “other” class (consisting of CSF, pathologies, and other non-brain tissues), experimentation is carried out on several brain MR images of BrainWeb and IBSR databases. The comparative performance analysis is depicted in Figure 5 using box-and-whisker plot. The significance analysis is also presented in Table 3 using uniform distribution (t -StoRM) and without using uniform distribution (t -StNU) to model the “other” class, with respect to different quantitative indices. In this regard, it should be mentioned that the class “other” in t -StNU is modelled using $St-t$ distribution, instead of uniform distribution and hence, the brain MR image is modelled using a finite mixture of $St-t$ distributions.

From all the results reported in Table 3, it can be seen that the proposed method, using uniform distribution for the class “other”, attains lower p-values for all quantitative indices with respect to t -StNU, which are also statistically significant. Also, the qualitative results reported in Figure 5 establish the importance of using uniform distribution to model the “other” class, in terms of optimal segmentation as well as intensity inhomogeneity correction.

4.5. Importance of Rough Sets

To establish the importance of rough set based modifications in the proposed t -StoRM algorithm, experimentation is carried out on several brain MR images of BrainWeb and IBSR databases. The comparative performance analysis is depicted in Figure 5 using box-and-whisker plot. The significance analysis is presented in Table 3 both using (t -StoRM) and without using rough sets (t -StNRS) in the proposed algorithm, with respect to different quantitative indices. In this regard, it should be noted that the membership values of each pixel into different tissue classes, in the t -StNRS algorithm, are estimated using (15) and the parameters of the stomped- t distributions are updated using (28) and (30), instead of using (16), (31), and (32), respectively.

From the results reported in Table 3, it is observed that the proposed method with rough sets attains significantly lower p-values when compared with t -StNRS using both Wilcoxon signed-rank test and paired t -test, for all evaluation indices. Also, the qualitative results reported in Figure 5 establish the importance of using rough set based modifications in terms of optimal segmentation and bias field correction.

4.6. Performance of Different Bias Field Correction Algorithms

To find out the effectiveness of the proposed t -StoRM algorithm for bias field correction over state-of-the-art algorithms such as RC2 [4], N3 [44], SPM8 [2], FSL [20], ASeg [46], mEM [17], MICO [28], and BCFCM [1], experimentation is carried out on 18 images of BrainWeb and 18 images of IBSR

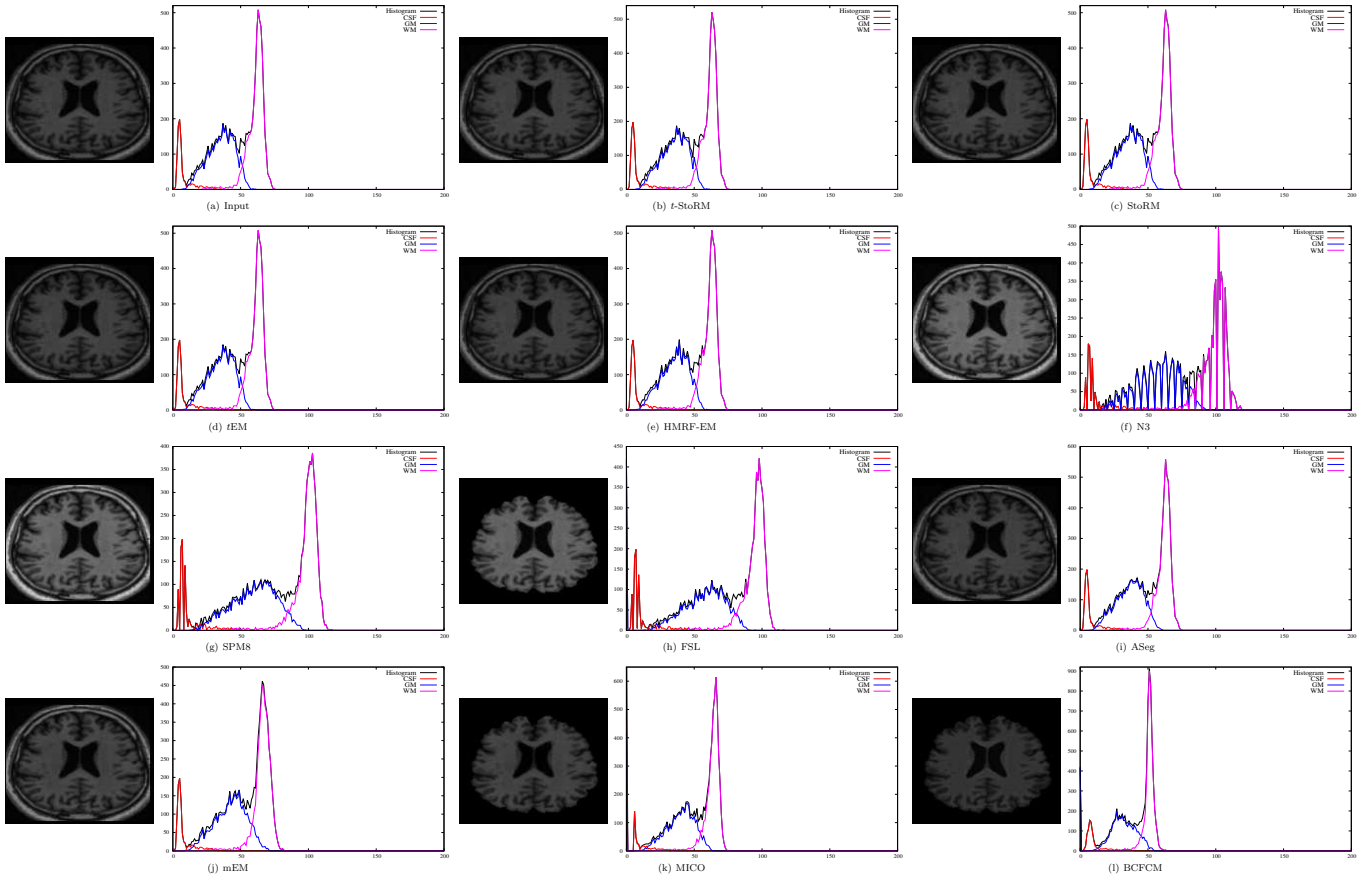


Figure 9. Input image of IBSR volume no. 8 and images restored by different algorithms, along with the intensity histograms.

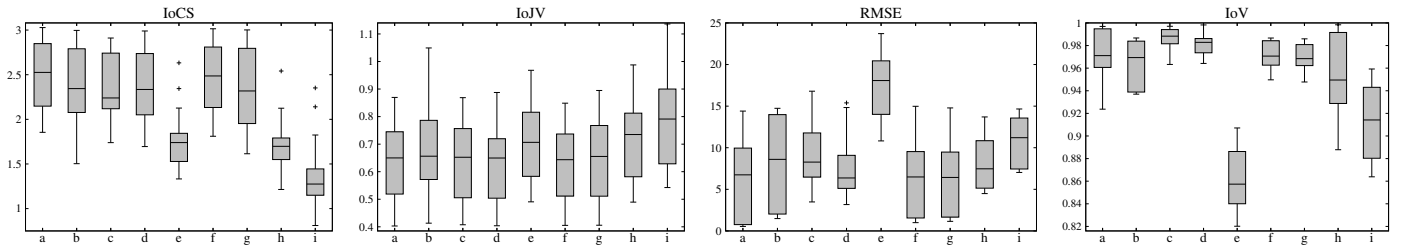


Figure 10. Box plot depicting the performance of proposed t -StoRM algorithm over state-of-the-art bias field correction algorithms on BrainWeb and IBSR databases. a) t -StoRM, b) RC2, c) N3, d) SPM8, e) FSL, f) ASeg, g) mEM, h) MICO, and i) BCFCM.

databases. The significance analysis with respect to Wilcoxon signed-rank test and paired t -test is presented in Table 4 for four quantitative indices, while the corresponding box plots are presented in Figure 10.

From the results reported in Figure 10 and Table 4, it can be seen that the proposed t -StoRM algorithm provides significantly better restoration than all existing algorithms with respect to IoCS index, considering 0.05 as the level of significance, irrespective of the statistical tests used. The proposed algorithm also attains significantly better restoration performance than RC2, FSL, MICO, and BCFCM for IoJV index. With respect to IoJV index, the proposed t -StoRM attains significantly better bias field correction results than mEM, when compared using paired t -test; while better but not significant (marked in *italics*) results, when compared using Wilcoxon signed-rank test. However, N3, SPM8, and ASeg provide better (marked in **bold**) restoration performance than the t -StoRM for IoJV index.

The proposed t -StoRM algorithm attains significantly better restoration performance than N3, FSL, MICO, and BCFCM for RMSE, irrespective of the statistical tests used. On the other hand, it achieves better results, but not significantly (marked in *italics*), compared to the SPM8, ASeg, and mEM with respect to RMSE, for both statistical tests. The proposed t -StoRM attains significantly better bias field correction results compared to RC2 algorithm for both RMSE and IoV values, when compared using paired t -test; while better but not significant results, when compared using Wilcoxon signed-rank test. With respect to IoV index, the performance of the proposed t -StoRM is significantly better than FSL, MICO, and BCFCM, while better but not significant compared to mEM. However, N3, SPM8, and ASeg provide better (marked in **bold**) restoration than the t -StoRM for IoV index.

The restored images produced by the t -StoRM, N3, SPM8, FSL, ASeg, mEM, MICO, and BCFCM are presented in Fig-

Table 4. Statistical Significance Analysis of the *t*-StoRM over Different Bias Field Correction Algorithms on BrainWeb and IBSR Databases

Algorithm	Mean	Std. Dev.	p-value	
			Wilcoxon	Paired <i>t</i>
IoCS				
<i>t</i> -StoRM	2.459574	0.472441	-	-
RC2	2.327793	0.528691	2.2E-03	0.0114
N3	2.339543	0.458204	1.4E-06	1.5E-05
SPM8	2.319970	0.550142	3.7E-09	6.6E-07
FSL	1.705142	0.333216	1.5E-11	4.9E-14
ASeg	2.422572	0.476535	3.1E-07	1.8E-06
mEM	2.302948	0.531196	4.8E-10	3.3E-06
MICO	1.673069	0.309817	1.5E-11	1.2E-15
BCFCM	1.315785	0.361947	1.5E-11	7.8E-16
IoJV				
<i>t</i> -StoRM	0.654734	0.233891	-	-
RC2	0.686928	0.233706	3.3E-03	0.0135
N3	0.654089	0.229192	0.6710	0.5344
SPM8	0.603430	0.175044	0.6710	0.8473
FSL	0.727979	0.233788	1.1E-08	8.0E-09
ASeg	0.652563	0.243083	0.8676	0.7676
mEM	0.676211	0.280335	0.0576	0.0270
MICO	0.738995	0.240806	7.3E-11	6.6E-11
BCFCM	0.818016	0.254304	2.0E-10	1.5E-09
RMSE				
<i>t</i> -StoRM	6.421026	5.037745	-	-
RC2	8.056794	5.285586	0.0770	0.0390
N3	8.974932	3.832738	7.9E-04	3.3E-04
SPM8	7.552986	3.794599	0.1419	0.0692
FSL	19.350462	3.755166	7.6E-06	1.2E-07
ASeg	6.624105	4.701238	0.3047	0.1755
mEM	6.509682	4.665884	0.3994	0.2961
MICO	8.253165	3.257652	0.0134	7.8E-03
BCFCM	10.802890	2.817903	2.7E-05	1.2E-06
IoV				
<i>t</i> -StoRM	0.969831	0.023606	-	-
RC2	0.925672	0.105151	0.1846	0.0449
N3	0.987196	0.008543	0.9976	0.9979
SPM8	0.981572	0.009669	0.9230	0.9662
FSL	0.863551	0.026627	3.8E-06	5.7E-10
ASeg	0.971130	0.012497	0.5000	0.6689
mEM	0.969379	0.012319	0.3509	0.4399
MICO	0.956159	0.035121	0.0333	0.0121
BCFCM	0.911376	0.034154	3.8E-06	2.5E-07

ures 6, 7, 8, and 9 for different bias fields, noise levels, and volumes. The restored images and corresponding intensity histograms reported in these figures confirm the fact that the proposed *t*-StoRM algorithm estimates bias field more accurately and restores images better than the state-of-the-art methods.

4.7. Performance of Different Segmentation Algorithms

This section compares the segmentation performance of the proposed *t*-StoRM algorithm with that of several state-of-the-art algorithms, namely, SPM8 [2], FSL [20], ASeg [46], mEM [17], MICO [28], KWFLICM [16], RFCM [33], rRFCM [37], BCFCM [1], DSFCM_N [49], ICFFCM [3], and FRFCM [27].

Table 5. Statistical Significance Analysis of the *t*-StoRM over Different Segmentation Algorithms on BrainWeb and IBSR Databases

Algorithm	Mean	Std. Dev.	p-value	
			Wilcoxon	Paired <i>t</i>
Dice Coefficient				
<i>t</i> -StoRM	0.865869	0.077326	-	-
SPM8	0.852910	0.083017	8.6E-04	1.0E-03
FSL	0.830975	0.072109	1.5E-11	1.4E-12
ASeg	0.663345	0.190230	1.5E-11	6.0E-09
mEM	0.604897	0.121859	1.5E-11	2.8E-14
MICO	0.853559	0.090479	0.0442	0.0300
KWFLICM	0.816302	0.114600	1.9E-06	1.3E-04
RFCM	0.858737	0.072801	3.9E-03	0.0171
rRFCM	0.838089	0.092067	7.3E-11	5.1E-06
BCFCM	0.850898	0.053002	7.3E-03	0.0122
DSFCM_N	0.802091	0.118710	1.5E-11	2.0E-06
ICFFCM	0.839345	0.099948	0.0346	4.9E-03
FRFCM	0.821467	0.108783	8.0E-10	1.1E-04
Sensitivity				
<i>t</i> -StoRM	0.898918	0.056861	-	-
SPM8	0.913043	0.038366	0.9256	0.8543
FSL	0.884582	0.054352	3.0E-06	4.5E-06
ASeg	0.769097	0.199141	1.6E-09	7.1E-05
mEM	0.664417	0.128373	1.5E-11	9.9E-14
MICO	0.885788	0.075168	0.0960	0.0384
KWFLICM	0.836768	0.103975	1.5E-11	2.8E-05
RFCM	0.888701	0.054362	1.3E-05	4.2E-05
rRFCM	0.880523	0.063241	2.0E-09	5.9E-06
BCFCM	0.850749	0.047603	7.3E-11	9.9E-14
DSFCM_N	0.831242	0.110633	1.5E-11	1.4E-05
ICFFCM	0.866048	0.099258	5.2E-03	4.5E-03
FRFCM	0.843112	0.104947	2.0E-10	7.3E-05
Specificity				
<i>t</i> -StoRM	0.981619	0.006873	-	-
SPM8	0.980365	0.006876	0.0228	0.0105
FSL	0.976818	0.006379	2.8E-10	5.9E-09
ASeg	0.934725	0.029774	1.5E-11	2.6E-12
mEM	0.931670	0.025061	1.5E-11	8.4E-15
MICO	0.979337	0.009837	0.0130	8.2E-03
KWFLICM	0.973961	0.014014	2.2E-08	8.2E-05
RFCM	0.979618	0.006808	1.9E-04	9.8E-04
rRFCM	0.976741	0.009781	1.5E-10	6.5E-06
BCFCM	0.978647	0.006816	7.7E-04	5.0E-04
DSFCM_N	0.972611	0.013798	1.5E-11	1.7E-06
ICFFCM	0.977687	0.011973	0.0148	1.7E-03
FRFCM	0.975682	0.012833	6.3E-10	8.4E-05

The significance analysis is presented in Table 5 with respect to Dice coefficient, sensitivity, and specificity values, while the box plots are presented in Figure 12.

From the results reported in Table 5 and Figure 12, it is observed that the *t*-StoRM provides significantly better segmentation results compared to FSL, ASeg, mEM, KWFLICM, RFCM, rRFCM, BCFCM, DSFCM_N, ICFFCM, and FRFCM, irrespective of the quantitative indices used. The performance of *t*-StoRM over SPM8 and MICO is also significantly better with respect to both Dice coefficient and specificity. With respect to sensitivity, the performance of *t*-StoRM over MICO is

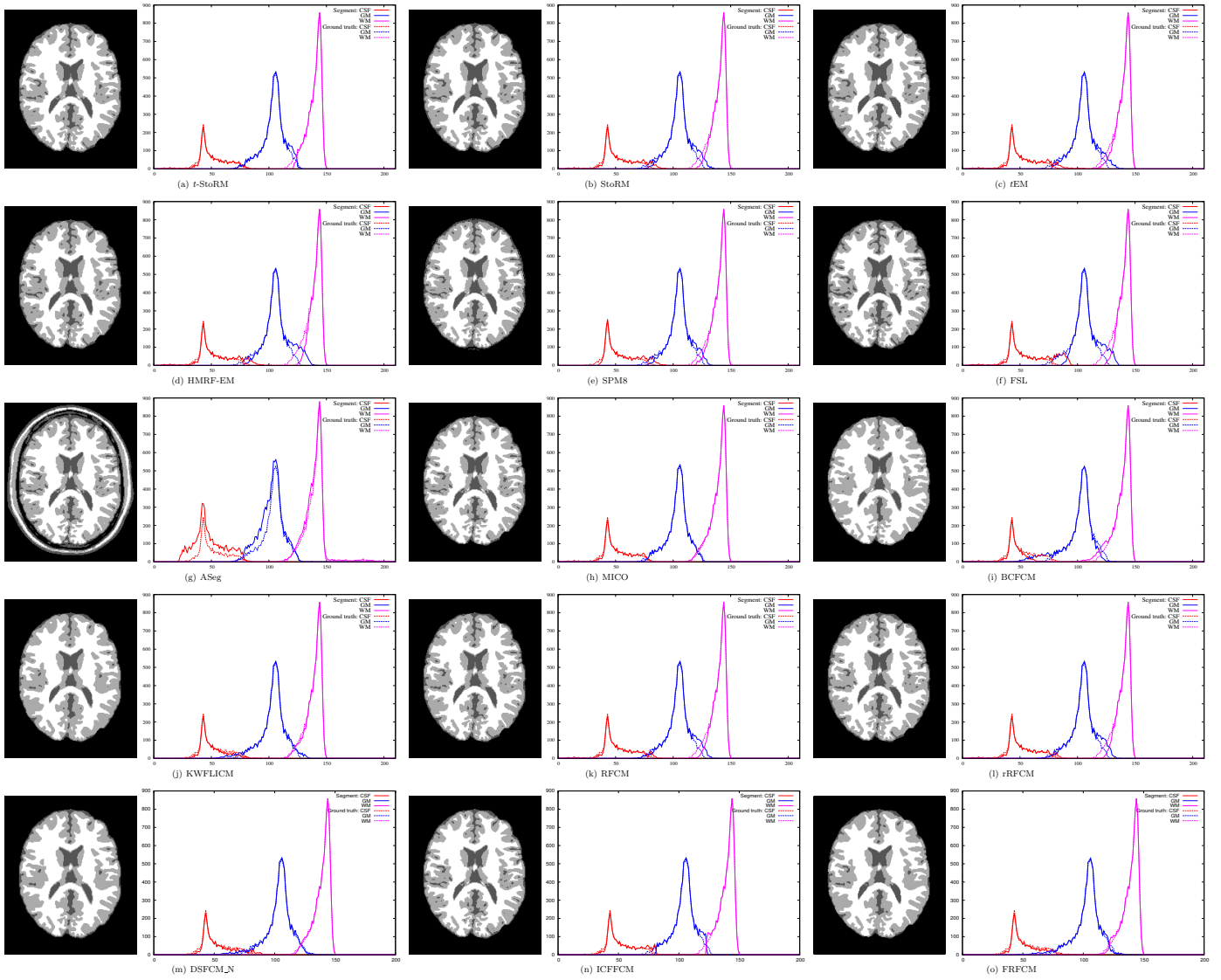


Figure 11. Segmented images by different segmentation algorithms on BrainWeb with 1% noise and 20% bias field, along with the intensity histograms.

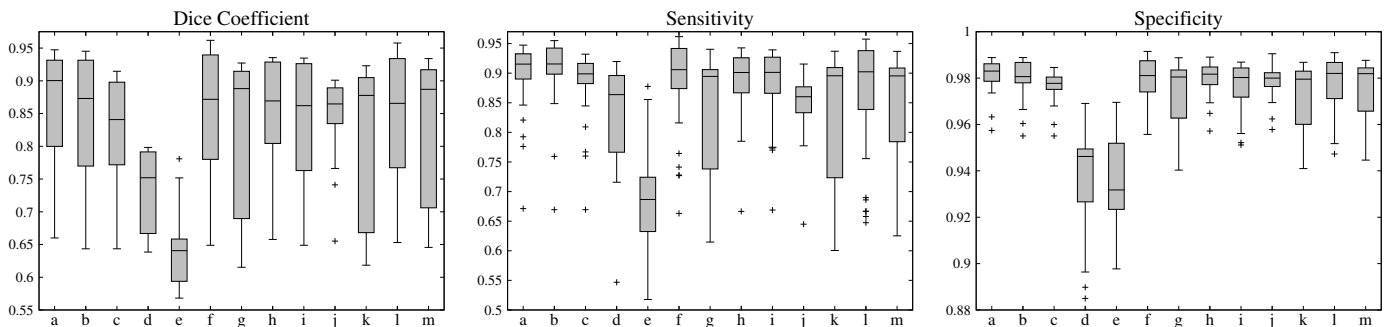


Figure 12. Box plot depicting the performance of t -StoRM over state-of-the-art brain MR image segmentation algorithms on BrainWeb and IBSR databases. a) t -StoRM, b) SPM8, c) FSL, d) ASeg, e) MEM, f) MICO, g) KWFLICM, h) RFCM, i) rRFCM, j) BCFM, k) DSFCM_N, l) ICFFCM, and m) FRFCM.

significantly better when compared in terms of p-values computed through paired- t test, while better but not statistically significant (marked in *italics*) when compared using Wilcoxon signed-rank test. However, the performance of the SPM8 is better, but not significant (marked in **bold**), than the proposed t -StoRM algorithm with respect to sensitivity.

The segmented images generated by the proposed t -StoRM algorithm, SPM8, FSL, ASeg, MICO, BCFM, KWFLICM, RFCM, rRFCM, DSFCM_N, ICFFCM, and FRFCM are reported in Figures 11, 13, 15, and 16 for different bias fields, noise levels, and volumes. The segmented images and corresponding intensity histograms reported in these figures infer

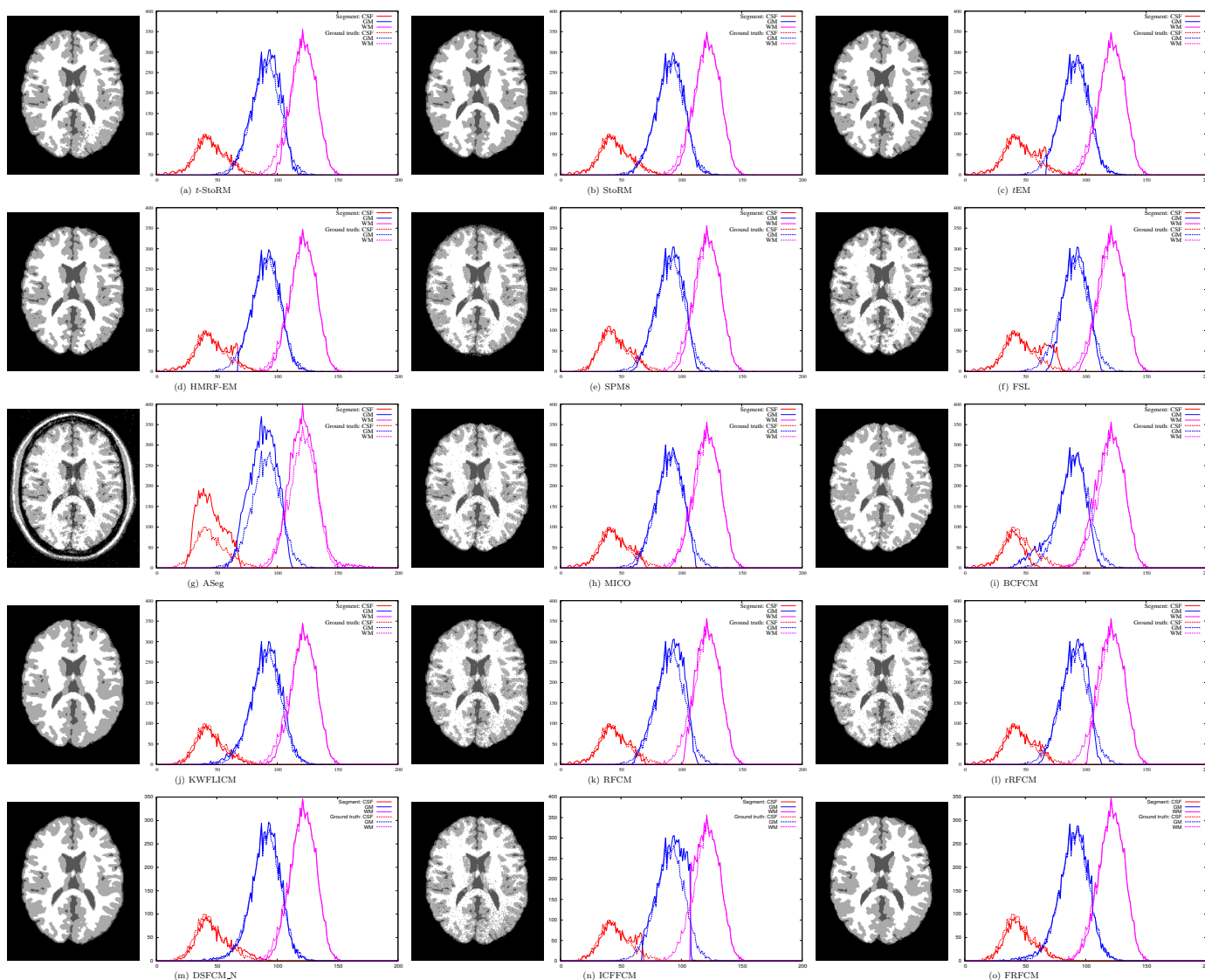


Figure 13. Segmented images by different segmentation algorithms on BrainWeb with 7% noise and 40% bias field, along with the intensity histograms.

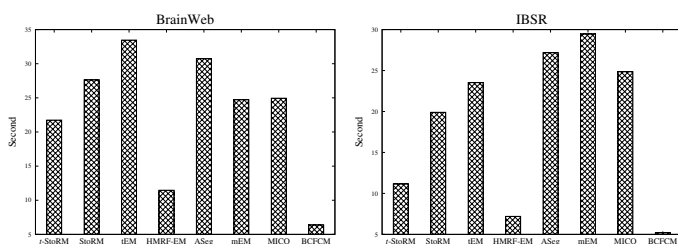


Figure 14. Run-time analysis of the proposed t -StoRM algorithm.

that the proposed t -StoRM algorithm generates more promising segmentation results than the state-of-the-art methods. The better performance of t -StoRM is obtained because of the fact that the $St-t$ distribution provides better intensity representation for tissue classes in brain MR images, which makes the t -StoRM perform well in brain MR image segmentation. Also, the integration of rough sets and $St-t$ distribution deals with uncertainty, vagueness, and incompleteness in tissue class definition and enables efficient handling of overlapping tissue classes.

The average run-time of the t -StoRM algorithm is com-

pared in Figure 14 with existing simultaneous segmentation and bias field correction algorithms for both BrainWeb and IBSR databases. From the figure, it is visible that the average run-time of the proposed t -StoRM is significantly lower compared to the StoRM, as the iterative t -StoRM converges faster to its optimum solution, compared to the StoRM. The average run-time of the t -StoRM is also significantly lower compared to the t EM, ASeg, mEM, and MICO algorithms. However, both HMRF-EM and BCFCM perform faster compared to the t -StoRM.

5. Conclusion

The problem of simultaneous segmentation and bias field correction in brain MR images requires special attention, as the bias field artifact deteriorates the performance of the segmentation algorithm. In this regard, the main contribution of this paper is the development of a new simultaneous segmentation and bias field correction algorithm, termed as t -StoRM. The merits of $St-t$ distribution is incorporated into the joint EM-HMRF

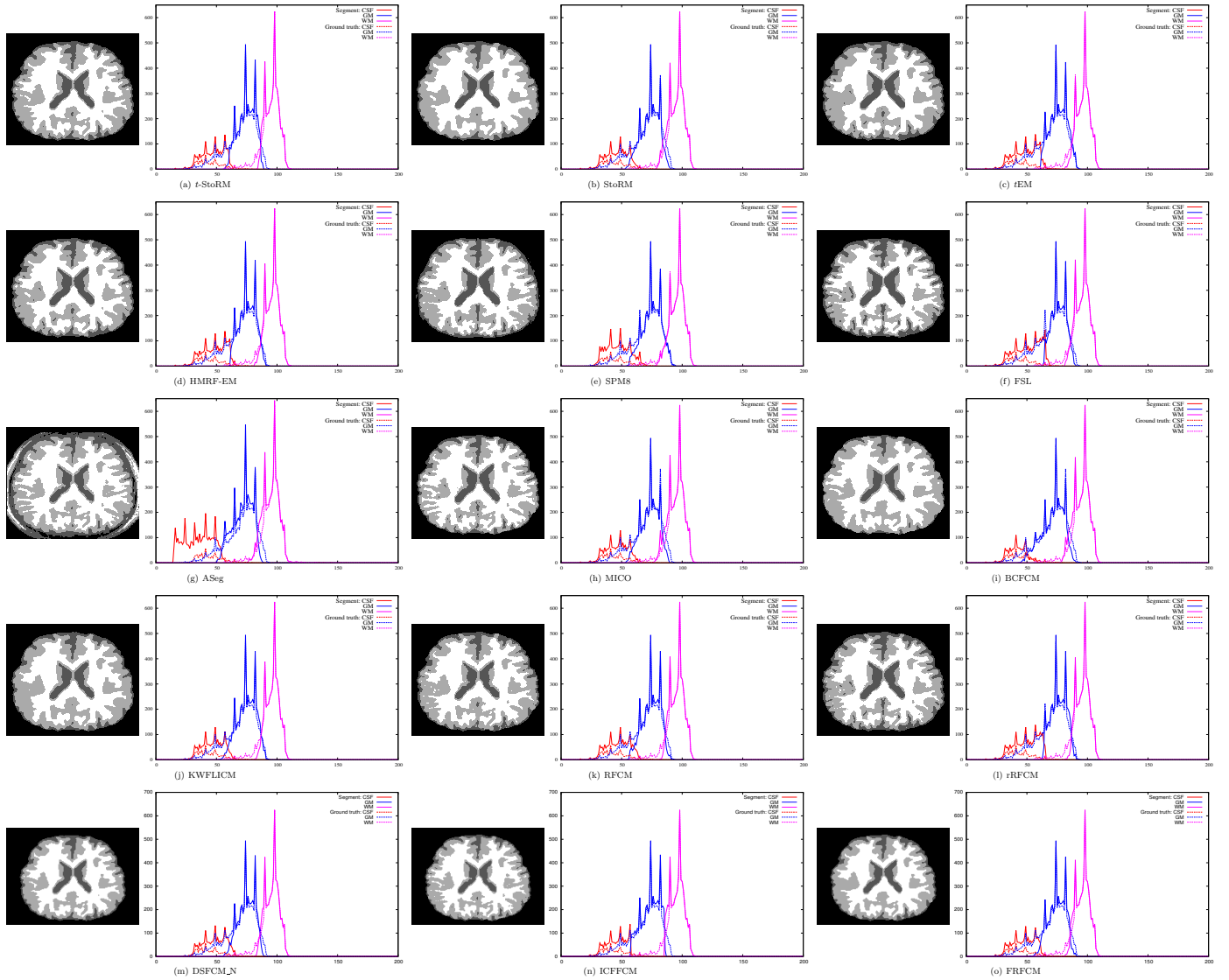


Figure 15. Segmented images by different segmentation algorithms on IBSR volume no. 1, along with the intensity histograms.

framework. Finally, the efficacy of the proposed algorithm is illustrated, along with a quantitative and qualitative comparison with related state-of-the-art algorithms, on a set of synthetic and real brain MR images.

The proposed framework has been able to achieve better image segmentation, as it utilizes the advantages of rough clustering with respect to brain MR image segmentation tasks. The representation of an image as a mixture of finite number of $St-t$ distributions and one uniform distribution has been able to provide a better modelling of the tissue intensity distributions in brain MR images, in presence of bias field artifact and noise. Moreover, the incorporation of a latent variable to measure the inlierness of each pixel with respect to tissue classes nullifies the need of a fixed parameter to measure the relative importance of lower approximation region, as done in StoRM [5]. In near future, the performance of this new probability distribution will be studied for other image processing tasks, such as image classification and registration. The multivariate extension of this probability distribution will be developed in order

to model high-dimensional data sets. The statistical properties of the probability distribution will also be explored in detail.

Acknowledgment

The authors would like to thank the editor-in-chief, the guest editor, and anonymous reviewers for their constructive comments and suggestions to improve the quality of the paper. This publication is an outcome of the R&D work undertaken in the project under the Visvesvaraya PhD Scheme of Ministry of Electronics and Information Technology, Government of India, being implemented by Digital India Corporation.

Appendix

Symbols

A	equivalence relation on universe \mathcal{U}
$\underline{A}(X)$	lower approximation region of set X

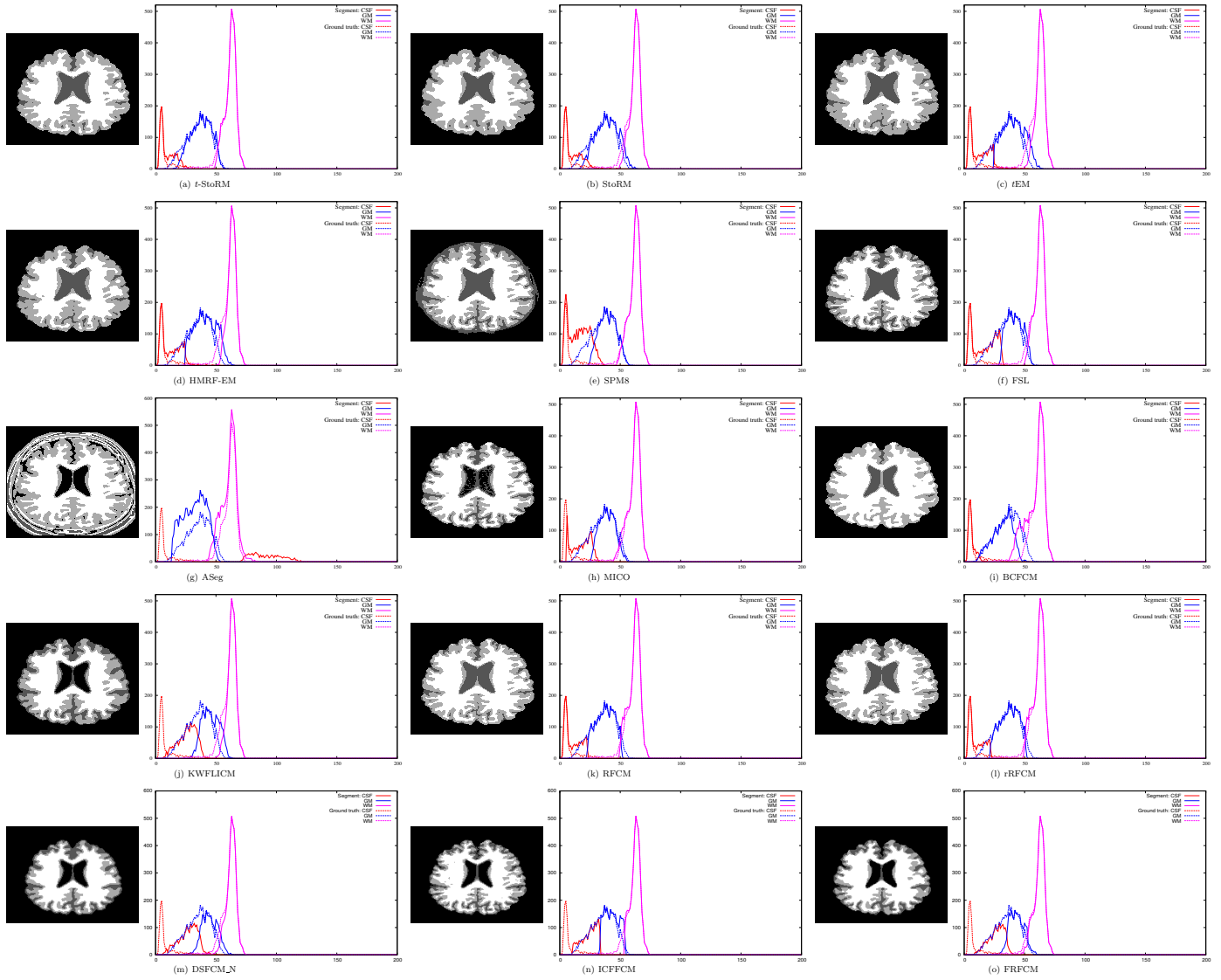


Figure 16. Segmented images by different segmentation algorithms on IBSR volume no. 8, along with the intensity histograms.

$\bar{A}(X)$	upper approximation region of set X	k_l	width parameter of Ω_l
$\langle \underline{A}(X), \bar{A}(X) \rangle$	rough set representation of set X	L	number of class labels in an image
a	scale parameter	\mathcal{L}	set of class labels in an image
$B(X)$	boundary region of set X	$(lu)_{il}$	expectation of $\log u_i$ given y_i and Ω_l
b_i	intensity inhomogeneity component in i th pixel	N	number of pixels in an image
\mathcal{C}	set of all possible cliques	\mathcal{N}_i	set of pixels neighboring pixel i
$D(\cdot)$	normalizing function in pdf of StN distribution	$n_i(l)$	number of neighbors of pixel i having label l
$E(\cdot)$	energy function	$O(\cdot)$	order of a function
$E_c(\cdot)$	clique potential	o_i	i th element of universe \mathbb{U}
F	low-pass filter	$Q(\cdot)$	expected complete data log-likelihood function
$\text{Gamma}(\cdot, \cdot)$	gamma distribution	$Q_{il}(\cdot)$	expected complete log-likelihood of pixel i to Ω_l
$G'_\Sigma(\cdot)$	Gaussian pdf with covariance matrix Σ	$Q_{2,il}(\cdot)$	expected log-likelihood of u_i given y_i and Ω_l

$Q_{3,il}(\cdot)$	expected log-likelihood of y_i given u_i and Ω_l	ν_l	degrees of freedom of class Ω_l
\bar{R}_i	mean residual of i th pixel	σ_l	scale parameter of class Ω_l
\mathcal{S}	set of indices in an image	τ_{il}	posterior probability that i th pixel belongs to Ω_l
StN(\cdot)	stomped normal distribution	$\Phi(\cdot)$	cdf of standard normal distribution
St- $t(\cdot)$	stomped- t distribution	$\phi(\cdot)$	pdf of standard normal distribution
\mathbb{U}	the universe of discourse	$\bar{\psi}^{-1}$	mean inverse covariance
\mathbb{U}/A	quotient set of \mathbb{U} by relation A	$\psi(\cdot)$	digamma function
$\langle \mathbb{U}, A \rangle$	approximation space consisting \mathbb{U} and A	$\psi'(\cdot)$	trigamma function
U_i	random variable of the inlierness of i th pixel	Ω_l	class having label l
u_i	latent variable of the inlierness of i th pixel	Ω_{other}	tissue class consisting of CSF, pathologies, and other non-brain tissues
u_{il}	expectation of u_i given y_i and Ω_l	\emptyset	empty set
v_i	intensity value of the i th pixel		
\tilde{v}_i	intensity of i th pixel of inhomogeneity-free image		
X_i	random vector of class label of i th pixel		
x_i	class label of the i th pixel of the image		
$x_{\mathcal{N}_i}$	set of class labels of pixels neighboring pixel i		
Y_i	random vector of log-transformed intensity of i th pixel		
y_i	log-transformed intensity value of the i th pixel		
\tilde{y}_i	log-transformed inhomogeneity-free intensity of i th pixel		
z_{il}	normalized variable of the StN distribution corresponding to i th pixel and class Ω_l		
$\hat{\alpha}$	estimate of the parameter α		
β_i	log-transformed bias field component of i th pixel		
$\Gamma(\cdot)$	gamma function		
$\Gamma(\cdot, \cdot)$	upper incomplete gamma function		
$\Gamma'(\cdot, \cdot)$	derivative of upper incomplete gamma function		
$\gamma(\cdot, \cdot)$	lower incomplete gamma function		
$\gamma'(\cdot, \cdot)$	derivative of lower incomplete gamma function		
$\delta(\cdot)$	Kronecker's delta function		
δ_{il}	indicator variable of belongingness of pixel i to Ω_l		
ϵ_i	noise component in i th pixel		
$\theta^{(t)}$	estimate of the parameter θ at t th iteration		
λ	density of the uniform distribution		
μ_l	location parameter of class Ω_l		

References

- [1] M. N. Ahmed, S. M. Yamany, N. Mohamed, A. A. Farag, T. Moriarty, A Modified Fuzzy C-Means Algorithm for Bias Field Estimation and Segmentation of MRI Data, *IEEE Transactions on Medical Imaging* 21 (3) (2002) 193–199.
- [2] J. Ashburner, K. J. Friston, Unified Segmentation, *NeuroImage* 26 (3) (2005) 839–851.
- [3] X. Bai, Y. Zhang, H. Liu, Y. Wang, Intuitionistic Center-Free FCM Clustering for MR Brain Image Segmentation, *IEEE Journal of Biomedical and Health Informatics PP (PP)* (2019) 1–10.
- [4] A. Banerjee, P. Maji, Rough Sets for Bias Field Correction in MR Images Using Contraharmonic Mean and Quantitative Index, *IEEE Transactions on Medical Imaging* 32 (11) (2013) 2140–2151.
- [5] A. Banerjee, P. Maji, Rough Sets and Stomped Normal Distribution for Simultaneous Segmentation and Bias Field Correction in Brain MR Images, *IEEE Transactions on Image Processing* 24 (12) (2015) 5764–5776.
- [6] A. Banerjee, P. Maji, Rough-Probabilistic Clustering and Hidden Markov Random Field Model for Segmentation of HEP-2 Cell and Brain MR Images, *Applied Soft Computing* 46 (2016) 558–576.
- [7] A. Banerjee, P. Maji, Stomped- t : A Novel Probability Distribution for Rough-Probabilistic Clustering, *Information Sciences* 421 (2017) 104–125.
- [8] A. Banerjee, P. Maji, Spatially Constrained Student's t -Distribution Based Mixture Model for Robust Image Segmentation, *Journal of Mathematical Imaging and Vision* 60 (3) (2018) 355–381.
- [9] J. Besag, On the Statistical Analysis of Dirty Pictures, *Journal of the Royal Statistical Society, Series B* 48 (3) (1986) 259–302.
- [10] Y.-T. Chen, A Level Set Method Based on the Bayesian Risk for Medical Image Segmentation, *Pattern Recognition* 43 (2010) 3699–3711.
- [11] C. A. Cocosco, V. Kollokian, R. K.-S. Kwan, G. B. Pike, A. C. Evans, BrainWeb: Online Interface to a 3D MRI Simulated Brain Database, *NeuroImage* 5 (4) (1997) 425.
- [12] D. L. Collins, A. P. Zijdenbos, V. Kollokian, J. G. Sled, N. J. Kabani, C. J. Holmes, A. C. Evans, Design and Construction of a Realistic Digital Brain Phantom, *IEEE Transactions on Medical Imaging* 17 (3) (1998) 463–468.
- [13] F. Dong, J. Peng, Brain MR Image Segmentation Based on Local Gaussian Mixture Model and Nonlocal Spatial Regularization, *Journal of Visual Communication and Image Representation* 25 (5) (2014) 827–839.
- [14] D. Dubois, H. Prade, *Fuzzy Sets and Systems: Theory and Applications*, Academic Press, New York, 1980.
- [15] Q. Ge, L. Xiao, J. Zhang, Z. H. Wei, An Improved Region-Based Model with Local Statistical Features for Image Segmentation, *Pattern Recognition* 45 (2012) 1578–1590.

- [16] M. Gong, Y. Liang, J. Shi, W. Ma, J. Ma, Fuzzy C-Means Clustering With Local Information and Kernel Metric for Image Segmentation, *IEEE Transactions on Image Processing* 22 (2) (2013) 573–584.
- [17] R. Guillemaud, M. Brady, Estimating the Bias Field of MR Images, *IEEE Transactions on Medical Imaging* 16 (3) (1997) 238–251.
- [18] A. E. Hassanien, A. Abraham, J. F. Peters, G. Schaefer, C. Henry, Rough Sets and Near Sets in Medical Imaging: A Review, *IEEE Transactions on Information Technology In Biomedicine* 13 (6) (2009) 955–968.
- [19] Y. He, M. Y. Hussaini, J. Ma, B. Shafei, G. Steidl, A New Fuzzy C-Means Method with Total Variation Regularization for Segmentation of Images with Noisy and Incomplete Data, *Pattern Recognition* 45 (2012) 3463–3471.
- [20] M. Jenkinson, C. F. Beckmann, T. E. J. Behrens, M. W. Woolrich, S. M. Smith, *FSL*, *NeuroImage* 62 (2) (2012) 782–790.
- [21] Z. Ji, G. Cao, Q. Sun, A Fuzzy Clustering Algorithm with Robust Spatially Constraint for Brain MR Image Segmentation, in: *Proceedings of the IEEE International Conference on Fuzzy Systems*, 202–209, 2014.
- [22] Z. Ji, J. Liu, G. Cao, Q. Sun, Q. Chen, Robust Spatially Constrained Fuzzy C-means Algorithm for Brain MR Image Segmentation, *Pattern Recognition* 47 (7) (2014) 2454–2466.
- [23] Z. Jia, Q. Suna, Y. Xiab, Q. Chena, D. Xiaa, D. Feng, Generalized Rough Fuzzy C-means Algorithm for Brain MR Image Segmentation, *Computer Methods and Programs in Biomedicine* 108 (2) (2012) 644–655.
- [24] J. T. Kent, D. E. Tyler, Y. Vard, A Curious Likelihood Identity for the Multivariate *t*-Distribution, *Communications in Statistics - Simulation and Computation* 23 (2) (1994) 441–453.
- [25] R. K.-S. Kwan, A. C. Evans, G. B. Pike, MRI Simulation-Based Evaluation of Image-Processing and Classification Methods, *IEEE Transactions on Medical Imaging* 18 (11) (1999) 1085–1097.
- [26] K. V. Leemput, F. Maes, D. Vandermeulen, P. Suetens, Automated Model-Based Bias Field Correction of MR Images of the Brain, *IEEE Transactions on Medical Imaging* 18 (10) (1999) 885–896.
- [27] T. Lei, X. Jia, Y. Zhang, L. He, H. Meng, A. K. Nandi, Significantly Fast and Robust Fuzzy C-Means Clustering Algorithm Based on Morphological Reconstruction and Membership Filtering, *IEEE Transactions on Fuzzy Systems* 26 (5) (2018) 3027–3041.
- [28] C. Li, J. C. Gore, C. Davatzikos, Multiplicative Intrinsic Component Optimization (MICO) for MRI Bias Field Estimation and Tissue Segmentation, *Magnetic Resonance Imaging* 32 (7) (2014) 913–923.
- [29] P. Lingras, C. West, Interval Set Clustering of Web Users with Rough K-Means, *Journal of Intelligent Information Systems* 23 (1) (2004) 5–16.
- [30] J. Luo, Y. Zhu, P. Clarysse, I. Magnin, Correction of Bias Field in MR Images Using Singularity Function Analysis, *IEEE Transactions on Medical Imaging* 24 (8) (2005) 1067–1085.
- [31] M. Majak, Universal Segmentation Framework for Medical Imaging Using Rough Sets Theory and Fuzzy Logic Clustering, in: *Information Technologies in Biomedicine*, Volume 3, vol. 283 of *Advances in Intelligent Systems and Computing*, 175–186, 2014.
- [32] P. Maji, S. K. Pal, RFCM: A Hybrid Clustering Algorithm Using Rough and Fuzzy Sets, *Fundamenta Informaticae* 80 (4) (2007) 475–496.
- [33] P. Maji, S. K. Pal, Rough Set Based Generalized Fuzzy C-Means Algorithm and Quantitative Indices, *IEEE Transactions on System, Man, and Cybernetics, Part B: Cybernetics* 37 (6) (2007) 1529–1540.
- [34] P. Maji, S. K. Pal, Maximum Class Separability for Rough-Fuzzy C-Means Based Brain MR Image Segmentation, *LNCS Transactions on Rough Sets IX* 5390 (2008) 114–134.
- [35] P. Maji, S. K. Pal, *Rough-Fuzzy Pattern Recognition: Applications in Bioinformatics and Medical Imaging*, Wiley-IEEE Computer Society Press, New Jersey, ISBN 978-1-118-00440-1, 2012.
- [36] P. Maji, S. Paul, Robust Rough-Fuzzy C-Means Algorithm: Design and Applications in Coding and Non-Coding RNA Expression Data Clustering, *Fundamenta Informaticae* 124 (1-2) (2013) 153–174.
- [37] P. Maji, S. Paul, Rough-Fuzzy Clustering for Grouping Functionally Similar Genes from Microarray Data, *IEEE/ACM Transactions on Computational Biology and Bioinformatics* 10 (2) (2013) 286–299.
- [38] T. M. Nguyen, Q. M. J. Wu, Fast and Robust Spatially Constrained Gaussian Mixture Model for Image Segmentation, *IEEE Transactions on Circuits and Systems for Video Technology* 23 (4) (2013) 621–635.
- [39] N. Otsu, A Threshold Selection Method from Gray-Level Histograms, *IEEE Transactions on Systems, Man, and Cybernetics* 9 (1) (1979) 62–66.
- [40] Z. Pawlak, *Rough Sets: Theoretical Aspects of Reasoning about Data*, Kluwer Academic, Dordrecht, The Netherlands, ISBN 978-0-7923-1472-1, 1991.
- [41] D. L. Pham, J. L. Prince, An Adaptive Fuzzy C-Means Algorithm for the Image Segmentation in the Presence of Intensity Inhomogeneities, *Pattern Recognition Letters* 20 (1) (1999) 57–68.
- [42] A. Ribbens, J. Hermans, F. Maes, D. Vandermeulen, P. Suetens, Unsupervised Segmentation, Clustering, and Groupwise Registration of Heterogeneous Populations of Brain MR Images, *IEEE Transactions on Medical Imaging* 33 (2) (2014) 201–224.
- [43] N. Richard, M. Dojat, C. Garbay, Distributed Markovian Segmentation: Application to MR Brain Scans, *Pattern Recognition* 40 (12) (2007) 3467–3480.
- [44] J. G. Sled, A. P. Zijdenbos, A. C. Evans, A Nonparametric Method for Automatic Correction of Intensity Nonuniformity in MRI Data, *IEEE Transactions on Medical Imaging* 17 (1) (1998) 87–97.
- [45] S. M. Smith, Fast Robust Automated Brain Extraction, *Human Brain Mapping* 17 (3) (2002) 143–155.
- [46] W. M. Wells, W. E. L. Grimson, R. Kikinis, F. A. Jolesz, Adaptive Segmentation of MRI Data, *IEEE Transactions on Medical Imaging* 15 (4) (1996) 429–442.
- [47] S. Widz, K. Revett, D. Ślęzak, A Hybrid Approach to MR Imaging Segmentation Using Unsupervised Clustering and Approximate Reducts, in: D. Ślęzak, J. T. Yao, J. F. Peters, W. Ziarko, X. Hu (Eds.), *Proceedings of the 10th International Conference on Rough Sets, Fuzzy Sets, Data Mining, and Granular Computing*, vol. 3642, 372–382, 2005.
- [48] L. A. Zadeh, Fuzzy Sets, *Information and Control* 8 (3) (1965) 338–353.
- [49] Y. Zhang, X. Bai, R. Fan, Z. Wang, Deviation-Sparse Fuzzy C-Means With Neighbor Information Constraint, *IEEE Transactions on Fuzzy Systems* 27 (1) (2019) 185–199.
- [50] Y. Zhang, M. Brady, S. Smith, Segmentation of Brain MR Images Through a Hidden Markov Random Field Model and the Expectation-Maximization Algorithm, *IEEE Transactions on Medical Imaging* 20 (1) (2001) 45–57.